A NUMERICAL STUDY ON EFFECT OF RECTANGULAR SHAPED RIBS ARRANGED IN DIFFERENT PATTERNS ON THERMAL PERFORMANCE OF A SOLAR AIR HEATER DUCT

A THESIS SUBMITTED IN PARTIAL FULFILLMENT OF THE REQUIREMENTS FOR THE DEGREE OF

Master of Technology

in

Mechanical Engineering

By

MOHAMMED RAYED FAROOQUI

213ME3431

DEPARTMENT OF MECHANICAL ENGINEERING

NATIONAL INSTITUTE OF TECHNOLOGY ROURKELA

ROURKELA – 769008

JUNE-2015

A NUMERICAL STUDY ON EFFECT OF RECTANGULAR SHAPED RIBS ARRANGED IN DIFFERENT PATTERNS ON THERMAL PERFORMANCE OF A SOLAR AIR HEATER DUCT

A THESIS SUBMITTED IN PARTIAL FULFILLMENT OF THE REQUIREMENTS FOR THE DEGREE OF

Master of Technology

in

Mechanical Engineering

By

MOHAMMED RAYED FAROOQUI

213ME3431

DEPARTMENT OF MECHANICAL ENGINEERING

NATIONAL INSTITUTE OF TECHNOLOGY ROURKELA

ROURKELA – 769008

JUNE-2015

NATIONAL INSTITUTE OF TECHNOLOGY, ROURKELA

CERTIFICATE

This is to certify that the thesis entitled, "**A NUMERICAL STUDY ON EFFECT OF RECTANGULAR SHAPED RIBS ARRANGED IN DIFFERENT PATTERNS ON THERMAL PERFORMANCE OF A SOLAR AIR HEATER DUCT**" submitted by **Mr. Mohammed Rayed Farooqui** in partial fulfillment of the requirements for the award of Master of Technology Degree in **Mechanical Engineering** with specialization in **Thermal Engineering** at the National Institute of Technology Rourkela is an authentic work carried out by him under my supervision and guidance.

To the best of my knowledge, the matter embodied in the thesis has not been submitted to any other University/Institute for the award of any degree of diploma.

Date 01/June/2015

Dr. Manoj Kumar Moharana
Assistant Professor
Department of Mechanical Engineering
National Institute of Technology Rourkela
Rourkela – 769008

SELF DECLARATION

I, Mohammed Rayed Farooqui, Roll No. 213ME3431, student of M.Tech (2013-2015), Thermal Engineering of Department of Mechanical Engineering, National Institute of Technology Rourkela do hereby declare that I have not adopted any kind of unfair means and carried out the research work reported in this thesis work ethically to the best of my knowledge. If adoption of any kind of unfair means is found in this thesis work at a later stage, then appropriate action can be taken against me including withdrawal of this thesis work.

NIT Rourkela
01 June 2015

Mohammed Rayed Farooqui

ACKNOWLEDGEMENT

I would like to express my heartfelt sense of indebtedness and gratitude to my project guide Dr. Manoj Kumar Moharana (Assistant Professor, Department of Mechanical Engineering) for inspiring and guiding me towards the completion of my project titled as "A numerical study on effect of rectangular shaped ribs arranged in different patterns on thermal performance of a solar air heater duct".

I would also like to thank my batch mates who have assisted me in the progress of my project.

Finally, I express my sincere gratitude to all those who have directly or indirectly helped me in completing this project report.

Date 1/06/2015

Place NIT Rourkela

Mohammed Rayed Farooqui

ABSTRACT

This work is concerned with a two-dimensional numerical study done to predict the influence of transverse rectangular cross-sectioned ribs on a solar air heater's convective heat transfer properties. Solar air heater is a useful device that can be utilized to augment the temperature of air by extracting heat from solar energy. It is a rectangular duct consisting of an absorber plate on its top and heat falls only on the top of absorber plate. When ribs/baffles are introduced just beneath the absorber plate, there is a considerable alteration in the thermal performance of air flowing through the rectangular duct. A comparison was made between the results of thin (high aspect ratio) and square ribs arranged in three patterns, namely, single wall arrangement, staggered arrangement and in-line arrangement on two opposite walls. The Nusselt number variation with Reynolds number range 5000-24000 was checked at a fixed rib pitch (p) and height (e) values. Computational fluid dynamics (CFD) simulations were performed using commercially available software ANSYS FLUENT v15.0. The results were compared with the existing experimental ones while performing simulations under similar conditions. Two methods were used to calculate the average Nusselt number in which one method extracted the local Nusselt number at many points and on averaging these, gave the average Nusselt number and the other method resembled the one used in the existing experimental work. The results revealed that, as compared to smooth duct, the introduction of ribs led to a considerable augmentation in heat transfer. Good agreement was found between the existing experimental results and numerical output, when the second method was adopted to calculate the Nusselt number. However the Nusselt number calculated using method 1 yielded values lower than the existing ones. The results revealed that the thin ribs yielded better performance than the squared ones. Out of the three arrangements, the best thermal performance was given by thin inline ribs whose convective heat transfer coefficient was 1.83 times smooth duct's convective heat transfer coefficient

Keywords: Solar air heater, turbulent flow, Nusselt number, ribs, Reynolds number.

Contents

List of Figures

List of Tables

Nomenclature

A_s	Ribbed surface area, m^2
D_h	Duct hydraulic diameter, mm
e	Rib height, mm
f	Friction factor of roughened duct
f_0	Friction factor of smooth duct
H	Channel height (excluding thickness of absorber plate and insulated wall), mm
h_{avg}	Average heat transfer coefficient, W/m^2K
h_z	Local heat transfer coefficient, W/m^2K
k	Thermal conductivity (W/m-K)
L	Total length of the duct, mm
L_1	Duct inlet length, mm
L_2	Duct test length, mm
L_3	Duct exit length, mm
m	Mass flow rate of air, kg/s
p	Rib pitch, mm
q"	Constant heat flux, W/m^2
T_f	Bulk fluid temperature of fluid at a particular location, K
T_{pm}	Mean plate temperature, K
T_{fm}	Mean fluid temperature, K
t_b	Thin ribs thickness, mm
t_t	Square ribs thickness, mm
v	Velocity of air, m/s
W	Channel width, mm

Dimensionless parameters

e/D_h	Relative roughness height
e/H	Relative pitch
g/p	Relative groove position

Nu	Nusselt number of roughened duct
Nu_0	Nusselt number of smooth duct
Pr	Prandtl's number
p/e	Relative roughness pitch
p/H	Rib blockage ratio
Re	Reynolds number
St	Stanton number of roughened duct
St_o	Stanton number of smooth duct
W/H	Aspect ratio of duct

List of greek symbols

ε	Dissipation rate, m^2/s^3
ω	Specific dissipation rate, 1/s
η_{thermo}	Thermal Enhancement factor
Γ	Molecular thermal diffusivity, m^2/s
Γ_t	Turbulent thermal diffusivity, m^2/s
μ	Dynamic viscosity, kg/m-s
μ_t	Turbulent viscosity, Ns/m^2
ρ	Density, kg/m^3

List of Subscripts

f	Fluid
fm	Fluid mean
i	Inlet
o	Outlet
pm	Plate mean
w	Duct wall
0	Smooth

Chapter-1

Introduction

Augmentation of convective heat transfer of a rectangular duct with the help of baffles/ribs has been a common practice in the past few years. This concept is widely applied in enhancing the thermo-hydrodynamic efficiency of various industrial applications such as thermal power plants, heat exchangers, air conditioning components, refrigerators, chemical processing plants, automobile radiators and solar air heaters [1]. Solar air heater is a device used to augment the temperature of air with the help of heat extracted from solar energy. These are cheap, have simple design, require less maintenance and are eco-friendly. As a result, they have major applications in seasoning of timber, drying of agricultural products, space heating, curing of clay/concrete building components and curing of industrial products [2, 3].

The shape of a solar air heater of conventional application is that of rectangular duct encapsulating an absorber plate at the top, a rear plate, insulated wall under the rear plate, a glass cover over the sun-radiation exposed surface, and a passage between the bottom plate and absorber for air to flow in [4, 5]. The detailed constructional details of a solar air heater are shown in fig. 1.1.

Solar air heaters have higher thermal efficiency when the Reynolds number of air flow through their passage is 3000-21000 [3]. In this range, the duct flow is generally turbulent. Hence, all the research work pertaining to the design of an effective solar air heater involves turbulent flow. Conventional solar air heaters with all the internal walls being smooth usually have low efficiency. The solar air heater's internal surface can be artificially roughened by mounting certain ribs/obstacles of different shapes such as circular wires, thin rectangular bars, etc. periodically on the lower side of collector plate. This results in a considerable augmentation in the heat transfer rate, but at the same time leads to increase in friction factor thereby enhancing the pumping power requirements.

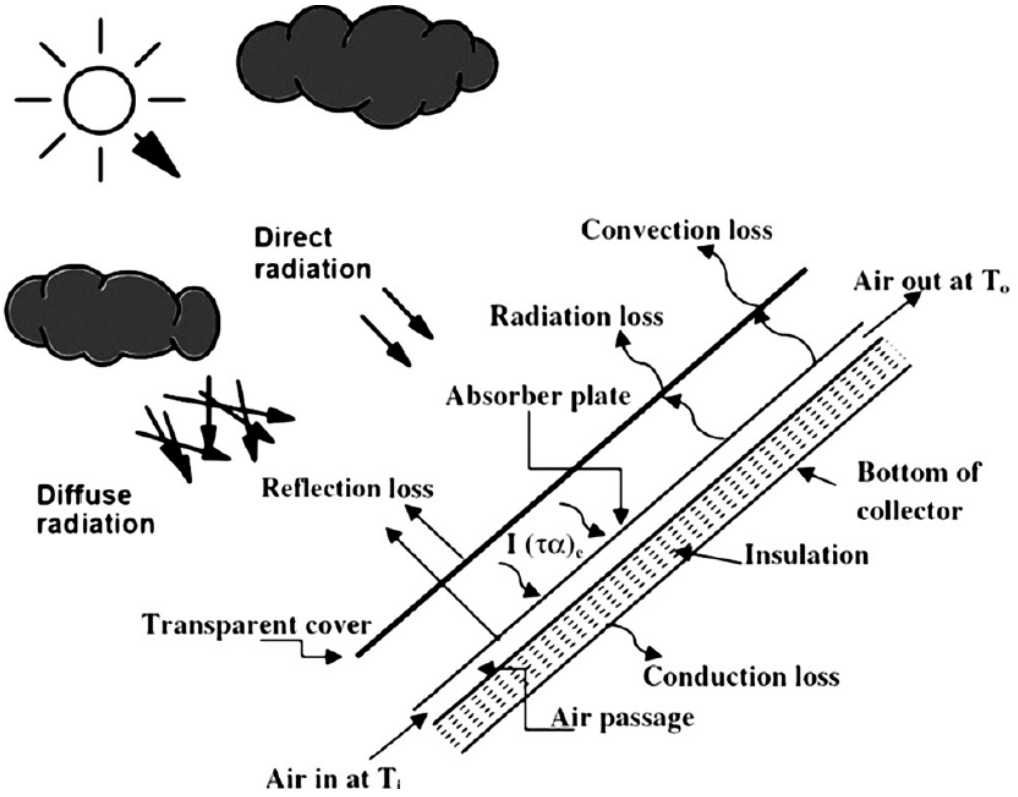

Fig. 1.1 Solar air heater constructional details [3]

It is a well-known fact that the friction factor and convective heat transfer coefficient of turbulent flow are highly dependent on the surface roughness of the duct through which they pass [6]. Hence, artificially roughened solar air heaters must be designed in such a manner that their performance yields higher convective heat transfer rates from absorber plate to air low roughness to air flow. Extensive research is being conducted in this field by many authors, whose work generally involves performing experiments or carrying out numerical simulations with different types, sizes and patterns of ribs/ baffles and finding the right parameters at which the heater gives optimal performance (minimum friction loss and maximum heat transfer). Some scientists, after performing research work on solar air heaters, develop a set of correlations for calculating Darcy's friction factor and Nusselt number in terms of operating and roughness parameters.

The mechanism by which heat transfer, between air and roughened absorber plate, increases is breakage of laminar sub-layer. The introduction of ribs leads to local wall turbulence and

breakage of laminar sub-layers leading to periodic flow reattachment and separation. Vortices are formed near these baffles, which leads to a significant rise in Nusselt number.

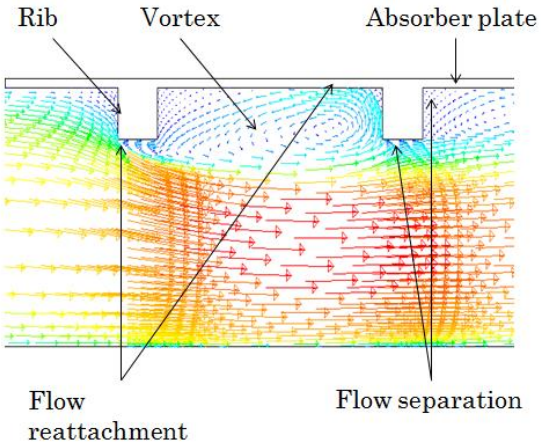

Fig. 1.2 Mechanism of augmentation of convective heat transfer by the introduction of ribs

As compared to experimental activities being carried on solar air heaters, very less numerical work has been done in this field. Numerical study of solar air heaters using CFD software is an excellent method to understand in detail how flow behaves under the presence of obstacles in solar air heaters. CFD results are more accurate as compared to experimental results. Other benefits of using CFD softwares are saving of time and less costs required to complete the work. Some commercially available CFD software packages are FLUENT, FLOVENT, CFX, STAR-CD and PHOENICS.

1.1 Introduction to turbulent flow

A laminar flow is characterized by regular and orderly motion of fluid elements. In this type of flow, viscous effects try to dampen out the disturbances of the fluid flow. Furthermore, in laminar flow, perturbations die out with fluid flow, but the reverse happens in case of turbulent flow, i.e. perturbations simply get amplified as the fluid flows. Turbulent flows occur when the inertial effects dominate the viscous forces.

The laminar velocity profile is approximately parabolic in nature, whereas the profile is much fuller in case of turbulent flows accompanied by a sharp decline in the vicinity of the wall. Turbulent flow regime can be generally divided into four different regions. The layer closest to wall is very thin and is popularly known as laminar sub-layer. Here, viscous forces are dominant

and the fluid flow behavior is almost the same as that of laminar flow. The next layer is called buffer layer, in which there is still an effect of viscous forces dominance but the flow somewhat becomes a bit turbulent. The buffer layer is followed by inertial sublayer, in which there is still some effect of turbulence, but not stronger. The turbulent (outer) layer is the core layer in which inertial forces become dominant over the viscous forces.

1.2 Introduction to Turbulence modelling

Additionally, turbulent flows possess certain distinguishing features such as randomness of transport (fluctuation of properties) variable with respect to time and space. The momentum exchange between particles of a fluid when it exhibits turbulent flow is high accompanied by strong mixing. Furthermore, turbulent flows contain wide range of length and time scales. Moreover, turbulent flow parameters are highly sensitive to initial conditions. For these reasons, it is very difficult to capture the physics of turbulent flow accurately in a single continuum simulation. The complexity exaggerates as the Reynolds number increases further.

Since there is high level of fluctuation of turbulent flows transport quantities with respect to time and space, conventional Navier-Stokes equation cannot be applied to capture their behavior. The addressed complexities can be overcome by a method called turbulence modelling. The set of mean flow equations are closed by this computational process. There are four different types of methods used in turbulence modelling

1. **RANS (Reynolds averaged Navier Stokes)/ RAS (Reynolds-average simulation):** The statistical average form of Navier-Stokes equation is considered to model the turbulent flows. Some of the different types of RANS models are Renormalization group RNG-k-ε model, SST (Shear Stress Transport) k-ω model, Standard RNG-k-ε model, Standard SST-k-ω model and Realizable k- ε model.
2. **DNS (Direct Numerical Simulation):** By resolving all scales of turbulence, the Navier-Stokes equation is numerically solved by this method.
3. **LES (Large Eddy Simulation):** This method involves solving large turbulent eddies with the help of governing differential equations, whereas the sub-grid scales are modelled.

4. **DES (Detached eddy simulation):** A combination of LES and RAS. The near-wall regions are treated with the help of RAS whereas the bulk flow regions are solved with the help of LES.

1.3 Objective of present work

The performance of solar air heaters are greatly altered by changing parameters such as flow velocity of air and the duct's internal surface roughness. The average Nusselt number is strongly dependent on these parameters. Hence this concept can be used in a positive way to enhance, between air flowing inside the duct and the absorber plate, convective heat transfer. For this reason, there has been an intense research in this field in the past. However most of these projects have been experimental and very less numerical work has been done. Numerical study of solar air heaters using CFD software is an excellent method to understand in detail how flow behaves under the presence of obstacles in solar air heaters. CFD results are more accurate as compared to experimental results. Other benefits of using CFD software are saving of time and lesser costs are required to complete the work. Hence, the objective of this work is to prove that CFD can be effectively used to design solar air heaters based on their thermal performance. This work deals with numerical study on the effect of transverse rectangular cross-sectioned thin baffles (high aspect ratio ribs). A detailed literature concerning work done on solar air heaters is presented in the next chapter. Moreover, it will be seen in open literature that no such work has yet been conducted. The present work motivation commences from the review so that the void in the literature can be filled. Hence, keeping in mind wide range of applications of solar air heaters and turbulent flow in the field of engineering, a dedicated work is required to understand the thermo-hydraulic behavior of these devices so that their efficiency can be improved such systems can be accurately designed.

1.4 Structure of thesis

This thesis contains five chapters. The first chapter starts with basics and explains the reason of carrying this work and ends up with a brief statement of the problem. The second chapter presents a detailed review of different experimental as well as numerical research works done on solar air heaters. The third chapter is concerned with problem formulation and lists down the governing equations along with explanation of boundary conditions, grid generation, numerical

techniques, grid independence tests and reduction of data. The fourth chapter titled as results and discussions presents the results of numerical simulation and explains them. The fifth chapter provides the conclusion and gives future insights of the concerned work.

Chapter 2

Literature Review

Prasad and Mullick [7] suggested that for the purpose of drying cereal grains, temperature increase of 3-6^{o}C was sufficient. They performed experiments on an unglazed rectangular duct, which was vented by an absorber plate at the top. Just beneath the absorber plate, protruding wires were provided, in order to study their effect on the friction characteristics and heat transfer properties of their solar air heater. They found that heat transfer coefficients agreed well with the existing theoretical correlations. They further commented that the effect of providing protruding wires beneath the absorber plate was that it helped to increase the unglazed collector's efficiency from 0.63 to 0.72, at a Reynolds number of 40,000.

Prasad and Saini [8] measured the performance of fully developed turbulent flow in an asymmetrically heated solar air heater duct which was provided with protruded wires just below the collector plate and derived the correlations for the calculation of average friction factor and average Stanton number. They found 6.3 % mean deviation of their friction factor results and 10.7 % of Nusselt number from the available data. They concluded that the addition of roughness to the absorber plate was to augment the heat transfer as well as the friction factor. They used two parameters to measure the performance of their solar air collector, which were relative roughness height and relative roughness pitch. As there was increment in the relative roughness pitch, the rate of heat transfer was observed to decrease with an increase in the value of friction factor, whereas the friction factor and the heat-transfer, both reduced with the enhancement in relative roughness pitch.

Prasad and Saini [9] attempted to optimize flow and roughness parameters so that they could increase heat transfer while keeping in mind minimum friction factor. They investigated the concerned properties in a range of parameters and found that for optimum thermo-hydraulic condition, a particular roughness Reynolds number always existed. They found that the Nusselt

number augmented with the increment in Reynolds number whereas reverse trend was observed in case of friction factor results. They further concluded that optimal conditions were obtained when the roughness height was slightly more than the thickness of transition sublayer. They constructed basis design curves that yielded parameters at which optimal thermos-hydraulic performance could be expected.

Liou and Hwang [10] conducted experiments on a rectangular duct, heated from the top, provided with three types of ribs, square, triangular and semicircular shapes. These were arranged transverse to the flow direction. The Reynolds number range was 7800-50000 and the rib height-to-hydraulic diameter ratio was 0.08. Fully developed flow conditions were established in their test section. They concluded that the three different configurations of solar air heater yielded comparable friction and heat transfer properties. Furthermore, the thermal performance in case of triangular and semicircular ribbed channels was less as compared to that of square ribbed channel.

Gupta et al. [11] did an experimental investigation on a solar air heater to find the fluid flow and thermal characteristics in the transitionally rough flow regime. The range of Reynolds number was 3000-18000 and the rectangular duct aspect ratio was varied from 6.8 to 11.5 whereas the relative roughness height was increased from 0.018 to 0.052. The value of relative roughness pitch was maintained constant at 10. They observed the behavior of Stanton number to be different in transitionally rough flow region as compared to that in fully rough flow regime. Furthermore, they developed a set of correlations that could predict the thermal and flow characteristics in the transitionally rough flow regime.

Saini and Saini [12] experimentally investigated fully developed turbulent flow in an asymmetrically heated and artificially roughened rectangular duct. The duct was covered with the help of an absorber plate that was incorporated with expanded metal mesh. The mesh relative long-way length (L/e) was varied from 25 to 71.87, the relative short-way length of mesh from 15.62 to 46.87 and the relative height of mesh (e/D_h) varied from 0.012 to 0.039. The experiments were conducted within the range of Reynolds number 1900 to 13000. The authors found that the change in the geometry of the expanded metal mesh had a strong influence on the thermal and frictional resistance of the solar air heater. From their experimental results, the

authors successfully created friction factor and Nusselt number correlations as a function of these parameters.

Karwa et al. [13] investigated experimentally the performance of their solar air heater when its collector plate was roughened with the help of repeated chamfered ribs. The rectangular duct aspect ratio was changed from 4.8 to 12.0 and the Reynolds number was varied from 3000 to 20000. The e/D_h range was 0.0141 - 0.0328, p/e range was 4.5-8.5 and chamfer angle range 15^o-18^o. Fully developed turbulent flow conditions were established in the rectangular duct's test section. The authors found that at chamfer rib angle of 15^o, the frictional resistance and heat transfer values were the highest. They further concluded that these were strongly dependent on the duct aspect ratio. The authors successfully developed correlations for the calculation of these parameters in terms of various parameters and observed that the highest Stanton number occurred with 20-25 as the Reynolds number range.

Verma and Prasad [14] conducted experiments on an artificially roughened rectangular duct heated from the top. Periodically repeated arrangement of thin wires, transverse to the flow direction, served the purpose of enhancing the roughness of the absorber plate. The thermo-hydraulic performance at optimal conditions was observed when the roughness Reynolds number was 24. They defined the thermo-hydraulic performance as $\eta_{thermo} = (\frac{St}{St_0})^3/(\frac{f}{f_0})$. They further concluded that the thermal performance parameter at optimal conditions was 71 %.

Murata and Mochizuki [15] numerically studied the influence of angled and transverse ribs on both laminar and turbulent flow in a solar air heater. The domain was a rectangular duct heated only on the top wall. The remaining walls were insulated. The angles of the ribs chosen were 60^o and 90^o. They found that in case of turbulent flow, high heat transfer coefficients spots were spotted at locations exactly between any two consecutive ribs. They further commented that the effect of the disturbances in case laminar flow was small as compared to that of turbulent flow. As a result, the heat transfer enhancement in case of laminar flow was very less as compared to that of turbulent flow.

Ahn [16] experimentally examined on a rectangular duct, the effect of five different shaped ribs on the thermal and fluid flow characteristics of turbulent flow (fully developed). The channel aspect ratio was 2.33 and was constant heat flux was supplied only at the top face of the test

section of the duct. The rib p/e and e/D_h values were fixed at 8 and 0.0476 respectively. The various geometries used as ribs were square, circular (wire), triangular and semicircular. They found that the triangular shaped rib gave maximum heat transfer coefficient and the square cross-sectioned ribs gave the highest friction factor value.

Momin et al. [17] conducted experiments on a v-shaped ribbed solar air heater to study its heat transfer and friction properties. The varied Reynolds number was from 2500 to 18000, angle of flow attack from 30 to 90^o and relative roughness height (e/D_h) from 0.02 to 0.034. The pitch of the arrangement was kept fixed at 10. The authors concluded that the presence of disturbances enhanced the heat transfer coefficient as well as the friction factor, on comparison to that of a smooth duct operating under the same flow conditions. It was inferred from the experimental results that the Reynolds number enhancement resulted in the augmentation in Nusselt number and a decrement in friction factor. The experimental results also revealed that as the Reynolds number increased, the Nusselt number enhancement rate was less as compared to the friction factor enhancement rate. Moreover, it was observed that the highest increase in friction factor and Nusselt number was 2.83 and 2.30 respectively at 60^o angle of attack. Additionally, the authors claimed that the v-shaped ribs gave the best thermo-hydrodynamic performance as compared to other shaped ribs. The authors were also successful in developing correlations for Nusselt number and friction factor as a function of different rib parameters and Reynolds number, where Reynolds number had a stronger influence as compared to other parameters.

Chandra et al. [18] experimentally studied friction and surface heat transfer performance of turbulent flow of air in a duct of square cross-section provided with transverse ribs on four, three, two and one wall. The experiments were performed within the Reynolds number range of 10,000 to 80,000. The ratio of channel length to the channel hydraulic diameter (L/D_h) was 20. The rib value of e/D_h and that of p/e were kept fixed at 0.0625 and 8 respectively. The authors observed that as the number of roughened walls increased, there was enhancement in friction factor and average Nusselt number.

Tanda [19] performed experiments on a rectangular cross-sectioned channel to study the effect of v-shaped ribs with attack angle 45^o or 60^o on fully developed turbulent flow. The ribs were both broken as well as continuous. In addition to v-shaped ribs, square cross-sectioned ribs effects were also studied separately. The author plotted the local heat transfer coefficients at different

Reynolds number in the turbulent flow region. The value of e/H, p/e and e/D_h of the duct ratios were varied from 0.15-0.25, 4-13.3 and 0.09-0.15 respectively. From the tests, it could be inferred that broken ribs had strong influence in increasing the Nusselt number. Furthermore, the author made conclusions that the highest heat transfer enhancement was observed at p/e = 4 and 8 with transverse broken ribs. Optimal conditions were obtained with broken transverse ribs at p/e = 4 and 13.3.

Sahu and Bhagoria [20] investigated experimentally the influence of 90^o broken ribs attached to a heated absorber plate in a solar dryer. They varied the Reynolds number from 3000 to 12000. The rectangular duct aspect ratio was fixed at 8, the value of e/D_h was 0.0338 and the roughness height e was 1.5 mm. The roughness pitch was varied from 10 to 30. The authors observed that at low Reynolds number, there was a sharp increase in Nusselt number value. The heat transfer coefficient was maximum at a pitch of 20 mm. Moreover, the authors claimed that a smooth duct could give better performance than the roughened channel at low Reynolds number. The experimental results led to the conclusion that the Nusselt number increased 1.25-1.4 times that of smooth duct, particularly at higher Reynolds number.

Chang et al. [21] conducted experiments on a rectangular duct provided with roughness on two opposite faces, in the form of scaled surfaces. Both laminar and turbulent flows were established separately and the flow directions were downward and forward. The experiments were set up in the range of Reynolds number 1500 – 15000. The values of p/e and e/H were kept fixed at 10 and 0.1 respectively. In the case of laminar flow, the Nusselt number increased 6.2-7.4 times and 7.4-9.2 times value of smooth duct for downward and forward flows respectively. Whereas in case of turbulent flow, the Nusselt number increased 3 times and 4.5 times value of smooth duct for downward and forward flows respectively. It was further observed that for the forward flow case, the friction factor was lower than that in the downward flow case. The authors concluded that better thermal performances would be obtained if the Reynolds number was maintained at values greater than 10,000.

Experiments were performed by Bhagoria et al. [22] using wedge shaped transverse ribs as a means of roughness on a rectangular channel solar air heater's absorber plate. The range of Reynolds number within which the tests were carried out was 3000-18000. The relative

roughness height (e/D_h), relative, (p/e) and rib wedge angle were varied from 0.015 to 0.033, to 12.12 and 8-15^o respectively.

Chaube et al. [23] carried out a numerical analysis of an artificially roughened solar air heater to study the roughness effect on friction factor and heat transfer. Commercially available FLUENT 6.0 software was used to solve the continuity and momentum equations computationally. They varied the Reynolds number from 3000-20000 and the turbulent model SST-k-omega was selected on the basis of predictions of various different turbulence models with available experimental results in literature. The simulations were performed on nine different types of rib shapes. The authors observed that the numerical results corresponding to 2-D and 3-D models had very less difference and hence the domain chosen was two-dimensional. They further stated that at regions exactly between two consecutive ribs, there was a large augmentation of heat transfer coefficient as a result of reattachment of flow with the absorber plate at these regions. At these locations, the turbulence intensity was the highest. The authors concluded that the highest heat transfer coefficient value was associated with chamfered ribs although rectangular rib of size 3X5 mm gave the best thermal performance.

Jaurker et al. [24] used artificial roughness in the form of transverse grooved ribs to experimentally investigate the effect of the disturbances on the friction factor and Nusselt number of a rectangular duct, heated only at the top. The range of parameters were Reynolds number 3000-21000, relative roughness pitch (p/e) 4.5-10.0, relative roughness height (e/D_h) 0.0181-0.0363, ratio of groove position to pitch 0.3-0.7. They concluded that grooved ribs gave higher Nusselt number (2.7 times of that of smooth duct) and a slightly more friction factor (3.6 times of that of smooth duct) as compared to those of transverse rectangular shaped ribs. At p/e value equal to 6, highest heat transfer occurred. At a value of groove position to pitch ratio 0.4, optimum conditions were established.

Wang et al. [25] using CFD software, numerically compared the performance of transpired solar air heater with respect to that of a smooth duct operating under the same conditions. The authors found that the transpired collectors gave much better thermal performance as compared to smooth ones. It could also be concluded from their work that CFD can be effectively applied to predict the friction and heat transfer characteristics of a solar air heater with some sort of roughness on its absorber plate.

Karmare and Tikekar [26] presented the results of experiments conducted on a rectangular channel of aspect ratio 10:1, whose absorber plate one side was roughened with the help of circular metal ribs arranged in staggered manner. The fluid flow and heat transfer characteristics were carefully studied at different Reynolds number (4000-17000), different relative roughness pitch (p/e) (12.5-36), different relative roughness height (e/D_h) (0.035-0.044) and different grit relative length (1-1.72). It was found that at duct roughness parameters $e/D_h = 0.044$, grit relative length = 1.72 and p/e = 17.5, optimal conditions were established. The friction factor and Nusselt number, at optimal conditions, were found to be 2.13 and 1.87 times those of smooth duct.

Layek et al. [27] attempted to numerically examine the artificial roughness effect on entropy generation in a solar air heater. An arrangement of repeated Chamfered ribs served the purpose of enhancing the roughness of an absorber plate placed at the top of the rectangular channel. From their numerical results, it could be inferred that as the relative roughness height (e/D_h) increased, the entropy generation declined. The entropy generation enhancement was observed to be minimum at relative groove position equal to 0.4, relative roughness pitch equal to 6 and chamfer angle equal to 18^o.

Aharwal et al. [28] attempted to utilize repeated squared ribs (splitted) with a gap attached on one surface of the absorber plate of a solar collector. The ribs were inclined to the direction of flow. The aspect ratio of the rectangular channel was 5.84. Experiments were performed under a range of roughness parameters gap width 0.5-2 and gap position 0.1667-0.667. The major roughness parameters such as p/e, e/D_h and angle of attack were kept invariable at 10, 0.0377 and 60^o respectively. 3000-18000 was the range of Reynold number. The Nusselt number and Fanning's friction factor were spotted to be 2.59 and 2.87 times those of a rectangular smooth duct, respectively. The optimal thermo-hydraulic conditions were found at a relative gap width and relative gap position of 1.0 and 0.25 respectively.

Experiments were performed by Pongjet and Thianpong [29] to predict friction loss and heat transfer behavior when air flows through a solar air heater being artificially roughened with the help of wedge shaped, triangular shaped and rectangular shaped ribs. Heat flux was applied only on the top wall of the test section of the duct. The aspect ratio of the duct was 15 with rib height as 6 mm and pitch as 40 mm. The Reynolds number was raised from 4000 to 16000. Two types of rib arrangements were designed, namely, staggered pattern and in-line configuration. The

authors concluded that higher heat transfer rates (2.6-4.4 times that of smooth duct) and friction factor were found with the in-line pattern. The highest enhancement in Nusselt number was observed when wedge rib (inclined downward to the direction of flow) was used. However, triangular shaped rib arranged in a staggered pattern gave the best thermal performance.

Saini and Saini [30] conducted experiments on a solar air heater provided with arc-shaped wired obstacles. The influence of arc angle and e/D_h on friction loss and heat transfer coefficient was studied when the Reynolds number was ranged from 2000 to 17000. The presence of arc shaped ribs gave rise to increase in Nusselt number by 3.8 times compared to that of smooth duct when the relative arc angle was 0.3333 and value of e/D_h was 0.0422. There was a less increment in the friction factor value.

Saini and Verma [31] investigated the effect of obstacles that were dimple shaped on the performance of a solar air collector. Reynolds number range was 2000 to 12000, range of e/D_h was 0.018-0.037 and range of relative pitch (p/e) was 8-12. Average Nusselt number and friction factor values were plotted with respect to Reynolds number. The authors spotted a considerable augmentation in the average heat transfer coefficient as a result of the introduction of these disturbances in the flow path. The highest value of Nusselt number was achieved at e/D_h equal to 0.0379 and p/e equal to 10. Whereas, the least value of friction factor was achieved at e/D_h equal to 0.0289 and p/e equal to 10.

Varun et al. [32] used a combination of transverse as well as inclined ribs on a collector plate of a solar dryer. Range of Reynolds number was 2000-14000, range of p/e was 3-8 and range of e/D_h was fixed at 0.03. Out of the range of different relative roughness pitches used, the one with a value of 8 yielded optimal efficiency. Furthermore, correlations for the calculation of frictional loss and Nusselt number were constructed.

Thianpong et al. [33] designed an experimental setup to examine the effect of isosceles triangular shaped ribs arranged in staggered and in-line patterns on the performance of a solar air heater. Range of Reynold number was 5000-22000, range of e/D_h was 0.0733-0.147, range of relative roughness pitch p/e was 5-10. Additionally, one arrangement of non-uniform ribs was also included for the examination. The authors observed that as compared to non-uniform ribs, uniform ribs performed well. In addition, in-line arrangement of ribs yielded larger friction factor

and Nusselt number as compared to that of the staggered arrangement under similar operating conditions. Moreover, it was inferred from the experimental results that inline rib arrangement with the highest e/D_h value gave maximum friction factor and Nusselt number enhancement. On the contrary, staggered arrangement of ribs combined with the least e/D_h yielded maximum thermal performance with an enhancement factor equal to 1.4.

Kumar and Saini [34] analyzed the effect of bent circular wire shaped ribs attached under a collector plate in a solar air heater. Range of Reynolds number was 6000-18000, relative roughness angle range was 0.333 to 0.666, e/D_h range was 0.0299 to 0.0426. The turbulence model that was used was Renormalization group (RNG) k-ε model. The thermos-hydraulic enhancement ratio was found to have the highest value at 1.7 for the different parameters examined.

An arrangement of periodically repeated W-shaped ribs was attached on a solar air heater's absorber plate by Kumar et al. [35] in order to experimentally analyze friction and thermal characteristics of air that flows inside the heater. Only the absorber plate was heated, wheare as the remaining sides were adiabatic. The rectangular duct's aspect ratio was 8:1. Reynolds number was ranged from 3000-15000, p/e was 10, e/D_h ranged 0.0168-0.0338 and the attack angle ranged from 30-75^o. The maximum enhancement ratio of friction factor and Nusselt number were 2.75 and 2.16 at 60^o angle of attack.

In Choompookham et al's [36] work, a combination of vortex generators of winglet type (WVGs) and wedge ribs was incorporated beneath the absorber plate of a solar air heater to study the frictional resistance loss and thermal behavior of fully developed fluid flow (turbulent) through the rectangular duct that was heated only at the top, that is at one side of the absorber plate. Staggered and in-line arrangements of ribs were followed. The channel aspect ratio was 10 with a height of 30 mm along with p/H = 1.33 and e/H = 0.2. The generation of longitudinal vortex flows was achieved by mounting WVGs with 60^o angle of attack at the entrance of the test duct. Range of Re was 5000-22000. The enhancement in friction factor and Nusselt number values was larger than those of WVGs alone. Moreover, the highest increment in Nusselt number was associated with the in-line wedge pointing downstream whereas optimal thermal behavior was achieved when upstream pointing staggered wedges were used as roughness elements.

With the help of CFD software, Karmare and Tikekar [37] developed a method to numerically investigate the impact of metal ribs, of circular, triangular and square cross-section with 60^o angle of attack mounted on the lower side of a solar air heater's collector plate, on flow and thermal behavior of fluid flow through the channel. The different parameters ranges were, Reynolds number 3600-17000, p/e = 17.5, l/s = 1.72 and e/D_h = 0.044. The CFD results were validated by performing experiments with the same operating conditions. There was a decent agreement between the numerical and experimental outputs. Furthermore, square ribs with angle of attack 58^o gave the highest convective heat transfer rate (1.3 times heat transfer rate of smooth duct).

An attempt to numerically investigate turbulent flow (fully developed) friction and convective heat transfer behavior of a solar air heater encapsulating v-shaped broken thin ribs at an angle of attack 60^o provided on two opposite heated walls (lower and upper duct walls) was carried out by Promvonge et al. [38]. The numerical method employed was finite volume method accompanied with SIMPLE algorithm to manage the coupling of pressure and velocity. Reynolds number range was 10,000 to 25,000. As the value of e/D_h was increased, average friction factor and Nusselt number also incremented. Optimal thermal performance parameter was 1.8 for roughness element having e/D_h value equal to 0.0725. Maximum convective heat transfer coefficient was observed to be approximately 4.0, particularly at low Reynolds number.

Sethi et al. [39] experimentally analyzed the influence of dimple shaped roughness elements with angular arrangement on friction and heat transfer behavior of a solar air heater. The disturbing elements were arranged periodically on the lower surface of its heated collector plate being placed on the top of the rectangular channel. The duct aspect ratio was 11 and the different range of parameters within which experiments were conducted were p/e = 10-20, Reynolds number 3600-18000, arc angle = $45 - 75^o$, e/D_h = 0.021-0.036. At e/D_h = 0.036, p/e = 10 and 60^o arc angle, highest convective heat transfer coefficient was achieved.

Sriromreun et al. [40] did experiments and numerical simulations to understand what happens to friction and thermal properties of asymmetrically heated fully developed fluid flow (turbulent flow) when z-shaped (zigzag) ribs were attached under a solar air heater's collector plate. The operating parameters and roughness parameters range were as, Reynolds number 4400-20400, rib-height-to-channel-height ratio (e/H) 0.1-0.3 and p/H ratio 1.5-3. Air stroked the baffles at an

angle of 45^o inclined to the ribs. The authors found that as compared to z-baffles out-phase, the z-baffles in-phase yielded much better thermal performance. The relationship between the numerical results and experimental observations was found to be in excellent agreement.

Promvonge et al. [41] roughened the surface of their square duct absorber plate by using finned tapes inclined at 30^o to the direction of fluid flow. They performed experiments with range of operating and roughness parameters as, Reynolds number 4000-23000, blockage ratio of fin (e/H) 0.1-0.3. At fin blockage ratio of 0.3, friction factor (6.7-10.9 times that of un-roughened duct) and convective heat transfer were maximum (5.9-6.3 times that of un-roughened duct) whereas at pitch ratio (p/H) of 1.0 and blockage ratio of 0.2, the thermos-hydraulic performance was optimum. The authors further concluded that the finned tape ribs gave much better thermal performance than that of twisted tape ribs. The highest thermal enhancement factor (TEF) was 1.8, but at smaller Reynolds number.

The previous work was validated by Promvonge et al. [42] when they numerically simulated a square duct of the same dimensions used in experimental work and operating under the same conditions. Finite volume method was employed to solve the governing equations and SIMPLE algorithm was utilized to manage coupling of pressure and velocity. At blockage ratio of 0.2 and pitch ratio of 1, the TEF was calculated as 1.95, which was the highest among all the other TEF's. However Nusselt number increment ratio was 4.5 at smaller Reynolds number.

With the help of CFD, Yadav and Bhagoria [43] performed numerical analysis on a smooth rectangular duct of aspect ratio 5. Five different turbulence models were used and their results involving friction factor and Nusselt number variation with Reynolds number were compared. ANSYS FLUENT version 12.1 software was used as a CFD code to resolve the governing equations numerically. In order to effectively manage pressure and velocity coupling, SIMPLE algorithm was employed. Range of Reynolds number was 3800-18000. RNG (Renormalization group) k-ε model gave the closest results to those of available correlations for a smooth duct.

This result encouraged Yadav and Bhagoria [44] to use RNG (Renormalization group) k-ε turbulence model so that they could experience what happened when thin wire-shaped ribs were mounted on the lower side of a solar air heater's absorber plate. The wires were located transverse to air flow. Range of Reynolds number was 3800-18000. The average Nusselt number

was maximum at p/e value equal to 7.14 and e/D_h value equal to 0.042 with a corresponding increment ratio of 2.31, at Reynolds number of 18000. As far as average friction factor was concerned, its maximum increment ratio was 0.0317 at p/e value equal to 7.14 and e/D_h equal to 0.042, at a Reynolds number of 3800. The highest TEF obtained was with p/e = 10.71 and e/D_h = 0.042.

Yadav and Bhagoria [45] attempted to use square cross-sectioned ribs in a solar air heater with a wide range of operating parameters and roughness parameters, Reynolds number 3800-18000, e/D_h = 0.021-0.042 and p/e = 7.14-35.71. The maximum TEF achieved was 1.88 at e/D_h = 0.042, p/e = 10.71 and at Re = 12000.

Prasad et al. [46] devised a novel experimental method to enhance their solar air heater's thermos-hydraulic performance by incorporating roughness elements on three sides rather than on one wall of the rectangular duct. The three walls (one top and two side walls) were uniformly heated while the bottom wall was insulated and smooth. The authors found 2-40 % and 20-75 % increment in friction factor and Nusselt number respectively when compared to the data of Prasad and Saini [8]. From the experimental results, it could be inferred that the new type of solar air heater gave much better performance than a solar air heater that was one-side heated and roughened. Average friction factor and Average Nusselt number correlations as a function of roughness and operating parameters were successfully developed.

Aharwal et al. [47] applied wedge shaped ribs with grooves on an a collector plate in order to raise the turbulence in air flow through a rectangular duct of aspect ratio 8, where constant flux was applied only on the top face of their absorber plate. The operating parameters and roughness parameters were experimentally ranged. Range of Reynolds number was 3000-18000, the range of wedge angle was 10^o to 25^o and range of relative groove position (g/p) was 0.4-0.8 and. The values of p/e and e/D_h were fixed at 8 and 0.033 respectively. The enhancement ratio of Nusselt number was 1.5-3 and that of friction factor was 2-3. Optimal conditions of thermal behavior were achieved when the relative groove position was 0.65 and the wedge angle was 15^o.

A series of v-shaped baffles (BVG) were used by Tamna et al. [48] to enhance wall roughness of a rectangular duct in order to test their influence on the thermo-hydrodynamic behavior on fully developed turbulent flow of air. The baffles were arranged in different manners, namely, one

wall, staggered and in-line on two opposite walls. Constant heat flux was given only on the upper wall. Range of Reynolds number was 4000 -21000, range of p/H was 0.5-2. Single values of b/H and attack angle were used as 0.25 and 45^{o}. As compared to single and staggered BVG, the BVG with in-line pattern gave higher convective heat transfer coefficient and friction factor. For all BVGs, maximum average convective heat transfer coefficient and average friction factor was obtained for smaller p/H ratios. The best thermal performance was however achieved with at p/H = 0.5 with single BVG, with the corresponding TEF value as 1.83.

Skullong et al. [49] described in their paper the effect of adopting a combination of groove and wavy-rib turbulators (ribs) in a solar air heater on its friction and thermal characteristics. They conducted experiments for Re range of 4000-21000, p/H of 0.5-2, and e/H = 0.25. Constant heat flux was supplied only on the test duct's upper wall. The wavy ribs were inclined at 45^{o} to the flow direction. The turbulators were arranged in three types of pattern, namely, one wall (upper wall only), staggered configuration and inline configuration on both lower and upper walls. Maximum average convective heat transfer coefficient and friction factor augmentations in the range approximately 4.4-7.69 and 14-134 were obtained with turbulators arranged in in-line manner at p/H = 0.5. The highest TEF was 1.75 and it was achieved with p/H = 0.5 at lower Reynolds number.

The works of various authors discussed so far focused mainly on ribs of low aspect ratios, geometries and pitch spacing ratios. This prompted Skullong et al. [1] to undertake an experiment on a solar air heater incorporated with thin ribs (ribs of high aspect ratios). The Reynolds number was raised from 5000-24000. The channel aspect ratio was 10 and the complete length of the duct was 2000 mm including a test portion length of 440 mm. The channel was 300 mm in width and 30 mm in height. The authors attempted to present a comparison of thermo-hydrodynamic performance between transverse thin and square ribs (ribs of low aspect ratios) arranged in three patterns, namely, single ribbed wall, staggered and in-line pattern on the lower and upper walls. As a result, six different configurations were achieved namely, single square rib, single thin ribs, staggered square ribs, staggered thin ribs, in-line square ribs and in-line thin ribs. Heat flux was given only on the upper wall of the rectangular duct test section, while the remaining surfaces remained insulated. Initially, in order to find which combination gave the best TEF, a fixed pitch length of 40 mm (p/H = 1.33) along with

square rib thickness of 6 mm and thin rib thickness of 0.5 mm were dimensions of the roughness elements established. It was found that the presence of ribs or disturbances had a strong influence on enhancing the friction factor as well as the convective heat transfer coefficient. The average Darcy's friction and average heat transfer characteristics were observed to be maximum for in-line thin ribs and minimum for single square ribs. As far as TEF, a parameter that takes into account both friction and heat transfer coefficient relative increment, was concerned, it was found to be the best, with a value of 1.3 at lower Reynolds number, for staggered thin ribs, whereas single square ribs gave the poorest TEF. The researchers extended their work by working experimentally on thin staggered ribs by varying rib blockage ratio (e/H) from 0.1 to 0.4, relative pitch (p/H) from 0.2 to 0.75. The authors concluded that at e/H = 0.4 and p/H = 0.5, highest average friction factor and average Nusselt number were achieved but the solar air heater gave the best TEF when the values of e/H and p/H were 0.2 and 0.75 respectively. Furthermore, the authors successfully developed a set of correlations that could be used to calculate average friction factor and average Nusselt number values, when Prandtl's number, Reynolds number, rib blockage ratio and relative pitch are the input parameters.

Chapter-3

Numerical Simulation

3.1 Problem Formulation

The present work is concerned with carrying out two-dimensional simulations on an artificially roughened solar air heater, through which air of air flows. The air heater internal surface was roughened with the help of transverse-square and thin (high aspect ratio) ribs. The ribs were arranged in different patterns namely one wall only, staggered and in-line on both lower and upper faces.

3.2 Computational domain

A rectangular section was considered. It consisted of three sections, test section of length L_2, entrance section of length L_1 and exit length of length L_3. The domain on which numerical simulations were performed was two-dimensional. It is because Chaube et al. [23] performed numerical simulations on their solar air heater of aspect ratio 7.5. They compared two-dimensional results with three dimensional results on the same geometry and did not find any considerable difference between the two. They explained their observation by claiming that for continuous transverse ribs, the secondary flow effect was negligible at higher duct aspect ratios. The geometry taken is similar to that of Skullong et al's [1] rectangular duct. Their rectangular duct was of length 2000 mm, width 300 mm and 30 mm with a test section length of 440 mm.

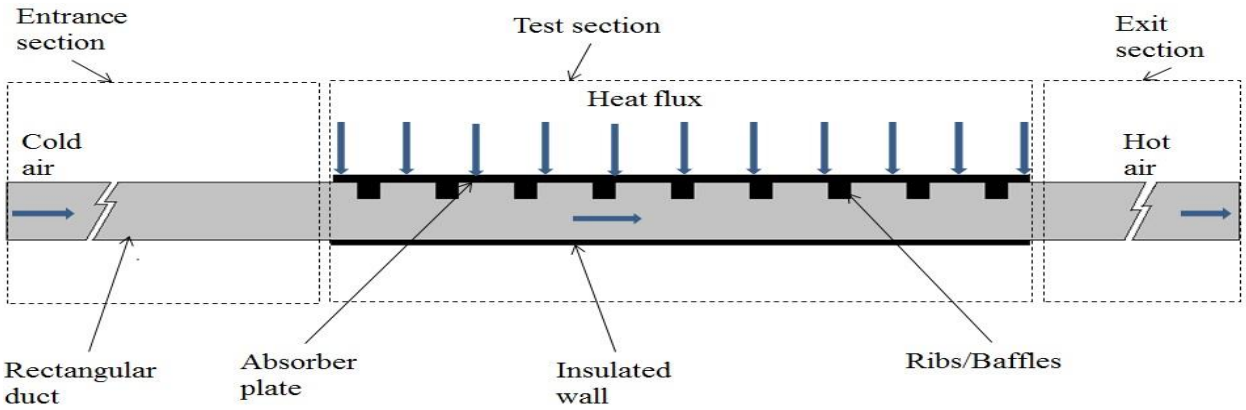

Fig. 3.1 Sketch of computational domain

Hence our domain test section length was 440 mm and its entrance and exit length dimensions were selected on the basis of ASHRAE recommendations, according to which an exit length more than $2.5\sqrt{WH}$ and entrance length more that $5\sqrt{WH}$ were compulsory to establish a fully developed flow in the test domain. Fig. 3.1 shows the geometry of the computational domain. The different rib arrangements employed for simulation are indicated in Fig. 3.2.

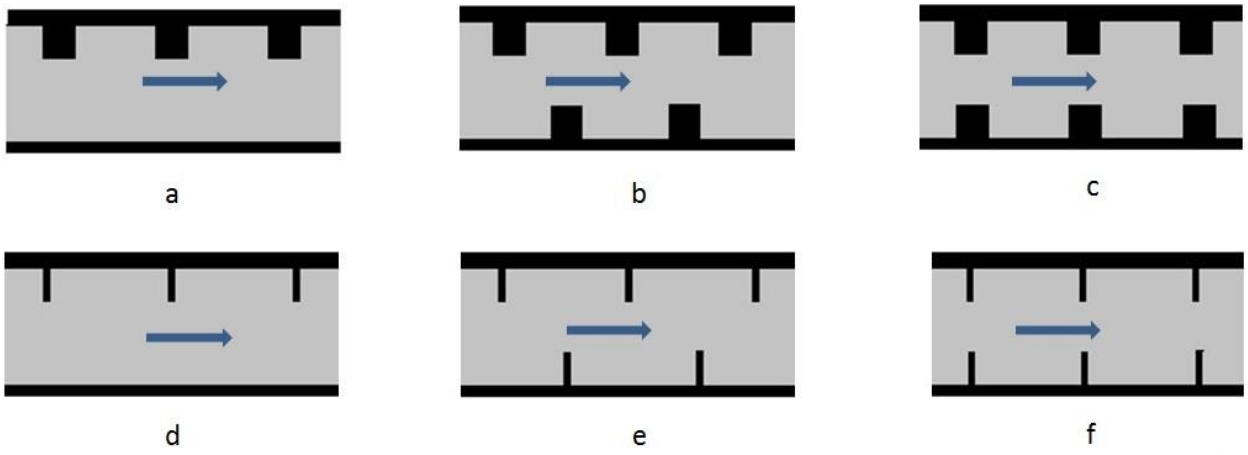

Fig. 3.2 Different arrangement of ribs namely (a) single square ribs, (b) staggered square ribs, (c) in-line square ribs, (d) single thin ribs, (e) staggered thin rib and (f) in line thin ribs

Table 3.1: Operating and Geometrical parameters used for CFD analysis

Operating and Geometrical parameters	**Value / Range**
Test length of duct, L_2	440 mm
Entrance length of duct L_1	500 mm
Exit length of duct L_3	240 mm
Duct height, H	30 mm
Duct width, W	300 mm
Duct hydraulic diameter, D_h	54.54 mm
Aspect ratio of duct, W/H	10
Constant heat flux, q"	1000 W/m^2
Range of Reynolds number	5000-23000

Repeated square ribs (t_t = 6 mm) and thin ribs (t_b = 0.5 mm) with an axial pitch of p = 40 mm characterized the roughness parameters of the test duct. Re was varied from 5000-23000 as this is the range in which solar air heaters particularly have higher efficiencies. Constant heat flux of value approximately 1000 W/m^2 was supplied only on the upper wall of the absorber plate. Simulations were performed assuming the flow to be steady. The operating and geometrical parameters used for computational analysis are listed in Table 3.1.

3.3 Governing differential equations

Continuity equation

$$\frac{\partial}{\partial x_i}\left(\rho u_i\right) = 0 \tag{3.1}$$

Momentum Equation

$$\frac{\partial}{\partial x_i}\left(\rho u_i u_j\right) = -\frac{\partial P}{\partial x_i} + \frac{\partial}{\partial x_j}\left[\mu\left(\frac{\partial u_i}{\partial x_j} + \frac{\partial u_j}{\partial x_i}\right)\right] + \frac{\partial}{\partial x_j}\left(-\rho\overline{u_i' u_j'}\right) \tag{3.2}$$

Energy equation

$$\frac{\partial}{\partial x_i}\left(\rho u_i T\right) = \frac{\partial}{\partial x_j}\left[\left(\Gamma + \Gamma_t\right)\frac{\partial T}{\partial x_j}\right] \tag{3.3}$$

where

$$\Gamma = \mu/\mathrm{Pr} \quad \text{and} \quad \Gamma_t = \mu_t/\mathrm{Pr}_t \tag{3.4}$$

3.4 Boundary conditions

On all the walls (including the roughened one) of the rectangular duct, no-slip boundary conditions were assigned. Constant heat flux of 1000 W/m^2 was decided to be the boundary condition at the upper wall of the absorber plate. At the inlet, uniform velocity with an inlet temperature of 300 K and at the exit, invariable pressure (atmospheric pressure) boundary conditions were assigned. All the other edges were assigned as walls with insulated boundary conditions, as shown in Fig. 3.3.

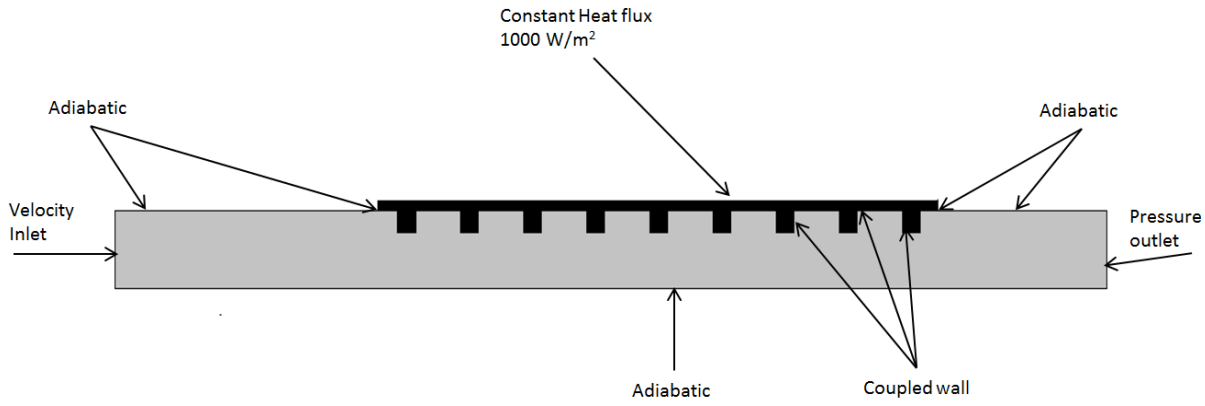

Fig. 3.3 Different boundary conditions assigned to edges of computational domain

3.5 CFD Modelling

Commercially available ANSYS FLUENT v 15.0 was the CFD software employed to solve the concerned general differential equations numerically. This software numerically simulates using FINITE VOLUME METHOD

3.6 Construction of Geometry

The geometry was constructed in commercially available software ANSYS Design Modeler v15.0. Firstly, an outline of the geometry without ribs was created in x-y plane with appropriate dimensions (in mm) and then surface was generated from the "built sketches" option. Then another sketch that involved the interface between absorber plate and fluid was developed. The surface initially created was split into two faces with the help of "face-split" option by choosing the second sketch as the tool geometry. The face-splitting option was followed by the generation of surfaces from the faces with the help of "create surface from faces" option. Finally, all the edges and surfaces were named accordingly.

3.7 Meshing of the domain

The meshing work was accomplished on commercially available ANSYS meshing software. The geometry created was imported in ANSYS meshing. The required number of divisions and the type of "bias" were assigned to each edge. In order to obtain regular rectangular shaped mesh cells with the best orthogonal quality, mapped facing option was activated. Finally, mesh was

generated by clicking on “Generate Mesh” button. Fig. 3.4 shows the meshed domain for different cases.

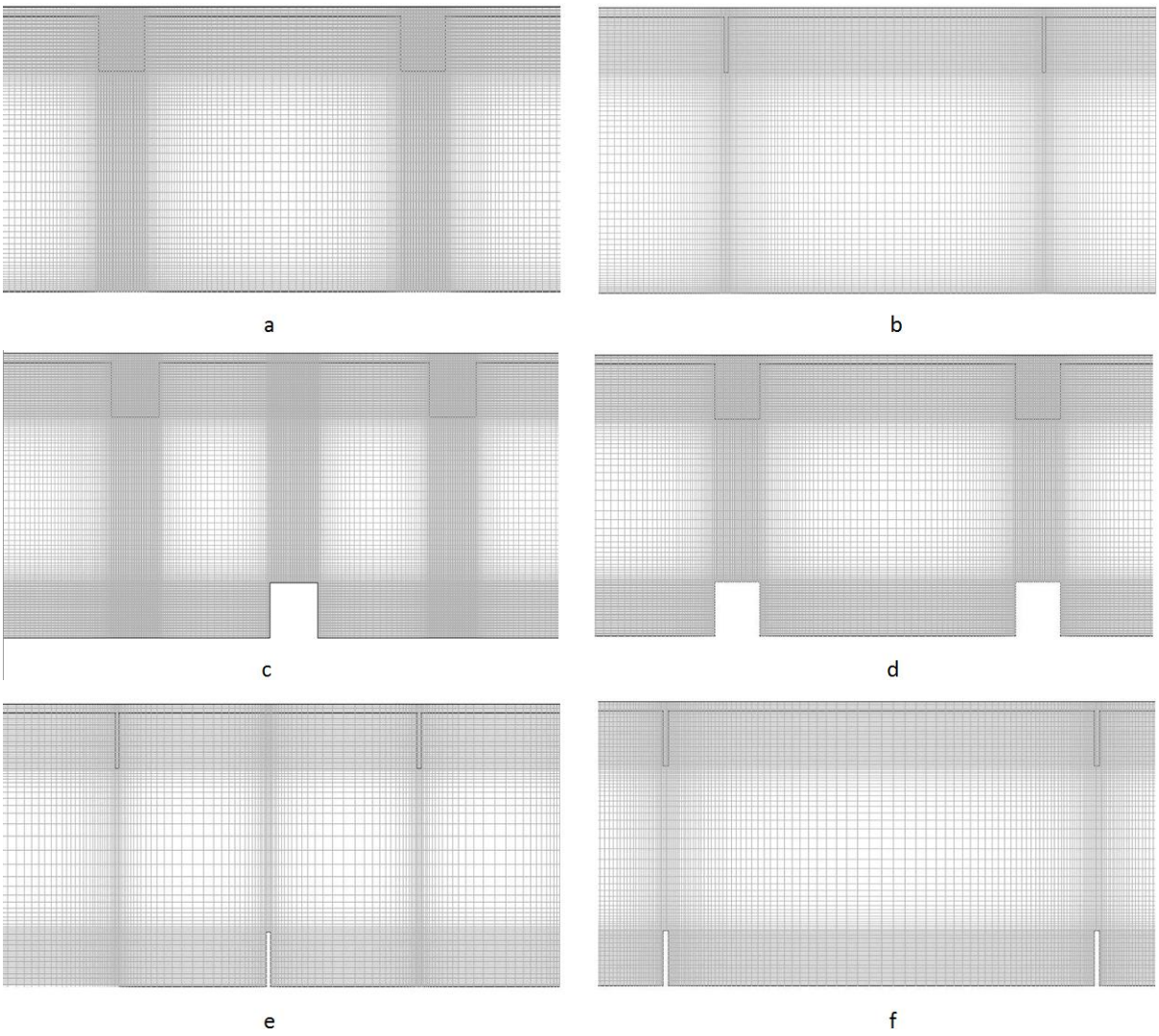

Fig. 3.4 Details of two-dimensional meshing of (a) single square ribs, (b) single thin ribs, (c) staggered square ribs, (d) in-line square ribs, (e) staggered thin ribs and (f) in-line thin ribs.

The meshed domain consisted mostly of non-uniform sized cells as shown in Fig. 3.4. Fine meshing was completed near the walls in order to solve the concerned governing differential equations accurately in the laminar sub-layers at these regions. The mesh size increased towards the center. The size of the grid was constant lengthwise in entrance and exit sections of the duct and it was ensured that the maximum aspect ratio of any grid did not exceed 10.

3.8 Set up and flow specification

The generated mesh was then exported to FLUENT where the different flow and physical properties were specified. The appropriate turbulent model was selected and the energy option was switched on. The working fluid was air and aluminum, because of its higher absorptivity, was the absorber plate. Their thermo-physical properties are mentioned in Table 3.2.

Table 3.2 Thermo-physical properties of aluminum as the absorber plate and air as the working fluid

Properties	**Working fluid (air)**	**Absorber plate (aluminum)**
Density, kg/m^3	1.1767	2719
Viscosity, kg/m-s	1.8582e-05	-
Specific heat (constant pressure), J/kg-K	1006.6	871
Prandtl number	0.714	-
Thermal conductivity, W/m-K	0.0262	202.4

Simulations were carried out under the following assumptions

1. The absorber and duct wall were assumed to be isotropic and homogenous.
2. Steady, turbulent and fully developed two-dimensional-flow.
3. The absorber plate and the duct wall thermal conductivity were temperature-independent.
4. Negligible heat losses and no radiation heat transfer.
5. At the junction of wall and fluid, no-slip boundary conditions were assumed.
6. The absorber plate and working fluid (air) properties were invariable at an average bulk temperature of 300 K.

3.9 Solution

The upwind scheme “second order upwind” was selected for momentum and energy equations. In order to couple velocity and pressure, the SIMPLE algorithm was applied. Temporal discretization was achieved using the solution method “Implicit integration”. Standard scheme was utilized to interpolate pressure and the relaxation factors for pressure, density, body forces, momentum and energy were maintained at 0.3, 1, 1, 0.7 and 1 respectively. A low convergence

criteria of 10^{-6} was chosen for the all the residuals in order to accurately predict different parameters. The solution was initialized by computing from the inlet using "Standard Initialization" option. After the completion of these settings, the iteration procedure was initiated by clicking on 'Run Calculation" button.

3.10 Reduction of Data

The parameters which were of key interest were local bulk temperature and local wall temperature along the axial direction. The local Nusselt number can be calculated with the help of these parameters.

Reynolds number

$$\mathrm{Re} = \frac{\rho v D_h}{\mu} \tag{3.5}$$

Local heat transfer coefficient is

$$h_z = \frac{q''}{(T_w - T_f)} \tag{3.6}$$

Average heat transfer coefficient equation is

$$h_{avg} = \frac{1}{L}\int_0^L h_z dz \tag{3.7}$$

During experimental methodology, a different method is adopted to measure the average heat transfer coefficient

$$h_{avg} = \frac{\dot{m} C_p (T_{out} - T_{in})}{A_s \left(T_{pm} - T_{fm}\right)} \tag{3.8}$$

where

$$T_{pm} = \frac{1}{12}\sum T_s \quad \text{and} \quad T_{fm} = \left(T_{in} + T_{out}\right)/2 \tag{3.9}$$

Local Nusselt number

$$Nu_z = \frac{h_z D_h}{k} \tag{3.11}$$

Average Nusselt number

$$Nu_{avg} = \frac{h_{avg} D_h}{k} \tag{3.12}$$

3.11 Grid Independence test

Selection of the best grid size is very important to achieve accurate results. Hence, grid independence tests were performed to predict appropriate grid dimensions to carry out the numerical simulations over a range of Reynolds number. The grid independence test was conducted at Re = 22500, since thickness of viscous laminar sub layers is the least at this Reynolds number. Hence, finding the right grid size at this Reynolds number would result in a grid size that would accurately predict heat transfer values for the entire Reynolds number range present in our simulation (Re = 5000-22500). In grid independence test, the total number of grids was increased till the difference in results between two consecutive grid sizes became negligible. At this moment, the grid size corresponding to the second last case of grid independence test was considered to be the best one and it was used for further simulations. Separate grid independence tests were conducted for different geometries.

3.12 Best turbulent model selection

In order to determine which turbulent model would most accurately yield numerical results, the following methodology was adopted. CFD calculations were performed on a smooth duct (without ribs) and the friction factor and Nusselt number variation with “Re” results were extracted from the simulation. The outputs were then compared with the experimental data of Skullong et al. [1]. Heat flux was applied only on the top wall of the test duct, whereas the other side remained insulated. Three different turbulent models, namely RNG-k-epsilon, SST-k-omega and Realizable-k-epsilon were chosen and their corresponding results in terms of Nusselt number alteration with Reynolds number were compared.

Chapter 4

Results and Discussions

In this project, a computational model was constructed to measure a solar air heater's thermal performance. It consisted of baffles/ribs just below its absorber plate. This section presents detailed results of the average convective heat transfer characteristics.

4.1 Selection of most appropriate turbulent model

For the smooth duct, the number of mesh cells was varied from 26280 to 186880 at a Reynolds number of 22500. It was observed in simulation results using SST-k-omega and RNG-k-epsilon turbulent model, there was less than 2% alteration in average Nusselt number after 143080 number of mesh cells. When the turbulent model was Realizable-k-epsilon, there was less than 2% alteration in average Nusselt number after 105120 number of mesh cells. Hence further simulations for different Reynolds number were performed using 143080 mesh cells with SST-k-omega and RNG-k-epsilon turbulent models and 105120 with Realizable-k-epsilon turbulence model. The Grid independence test results are represented in Fig. 4.1

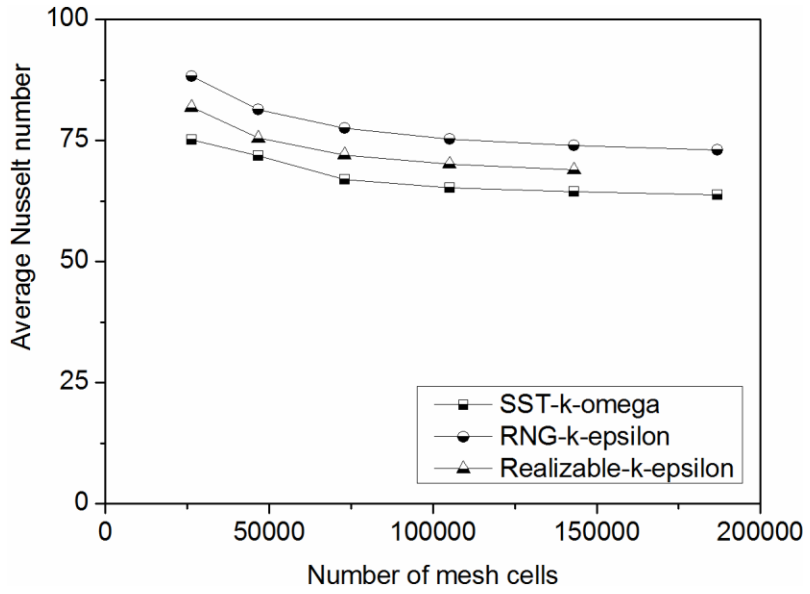

Fig. 4.1 Grid independence test results for selection of most appropriate turbulence model

Fig. 4.2 shows that as the Reynolds number incremented, the average Nusselt number increased for all the three turbulent models. The reason why this trend was observed was that as the Reynolds number increased, the flow became more turbulent (more dominance of inertial effects over viscous effects) and hence the heat transfer rate increased. Furthermore, it could be seen that the turbulent model that was the closest to Skullong et al. [1]'s output and theoretical results in the best manner was SST-k-omega. The error associated was less than 3 %. Hence, SST-k-omega turbulent model was used for simulating the roughened ducts.

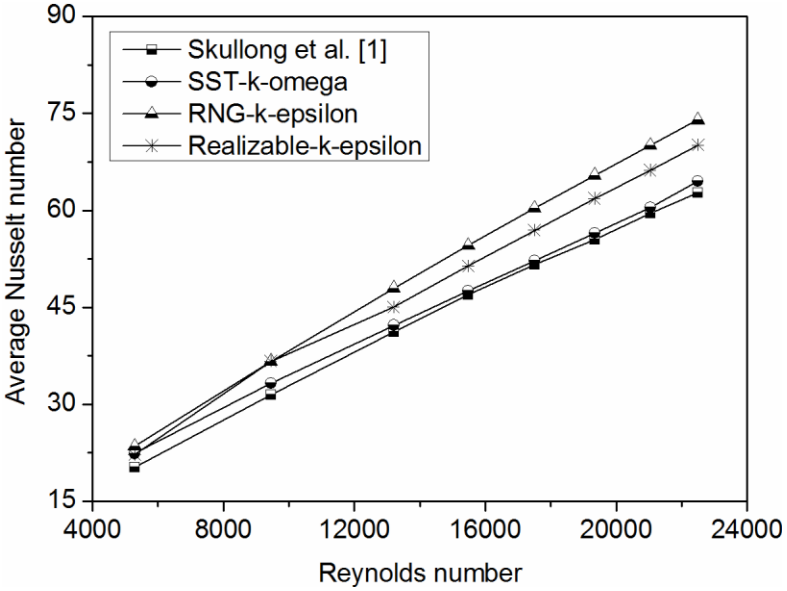

Fig. 4.2 Comparison of smooth duct results for different turbulent models

4.2 Numerical simulations on ducts with different shaped ribs

This section presents detailed results of average convective heat transfer characteristics of the heater, for different shaped ribs.

4.2.1 Grid Independence test results for all the different geometries

Figure 4.3 shows the results of grid independence tests conducted on different geometries. The turbulent model used was SST-k-omega for all the cases, since in the previous section it was proved that SST-k-omega most accurately simulated a solar air heater. The best mesh size was extracted from the Grid Independence test when there was less than 2 % variation in results on

further increasing the number of mesh cells after this mesh size. Table 4.1 gives the range in which the number of mesh cells was varied and the most appropriate number of mesh cells for each configuration.

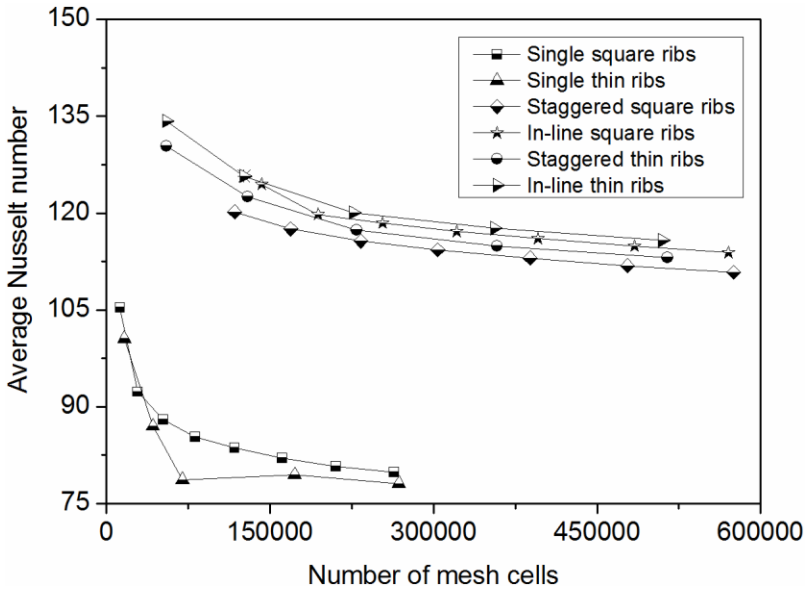

Fig. 4.3 Grid independence test results for different rib arrangements

Table 4.1 Grid Independence test results

Rib configuration	Range of mesh cells	Best number of mesh cells
Single square	12516 – 268396	210636
Single thin	16500 – 268366	172620
Staggered square	117644 – 575320	477864
In-line square	142316 - 570576	484284
Staggered thin	55048 – 514568	357962
In-line thin	54934 - 509856	355882

4.2.2 Simulation for different roughened ducts at different Reynolds number

The best grid sizes were obtained by performing grid independence tests whose results were explained in the previous section. The average convective Nusselt number was measured using two methods. The first method (method-1) is given by equation 3.7 and takes the average of all

the local Nusselt numbers along the test section length. The second method (method-2) used Eq. 3.8 and it is the most widely employed method of calculating Nusselt number in experimental works. The second method was used by Skullong et al. [1]. Fig. 4.4 clearly depicts the outcome of average Nusselt number alteration with Re for the geometries separately. As Re was raised, the average Nusselt number increased for all cases. The reason why this trend was observed was that as the Re was raised, the flow became more turbulent (more dominance of inertial effects over viscous effects) and hence the heat transfer rate increased.

There was a decent agreement when numerical outputs were compared with the experimental ones existing in the literature. Excellent matching between Nusselt numbers calculated using method 2 and the existing ones was observed for square ribs but good agreement was found in case of thin ribs.

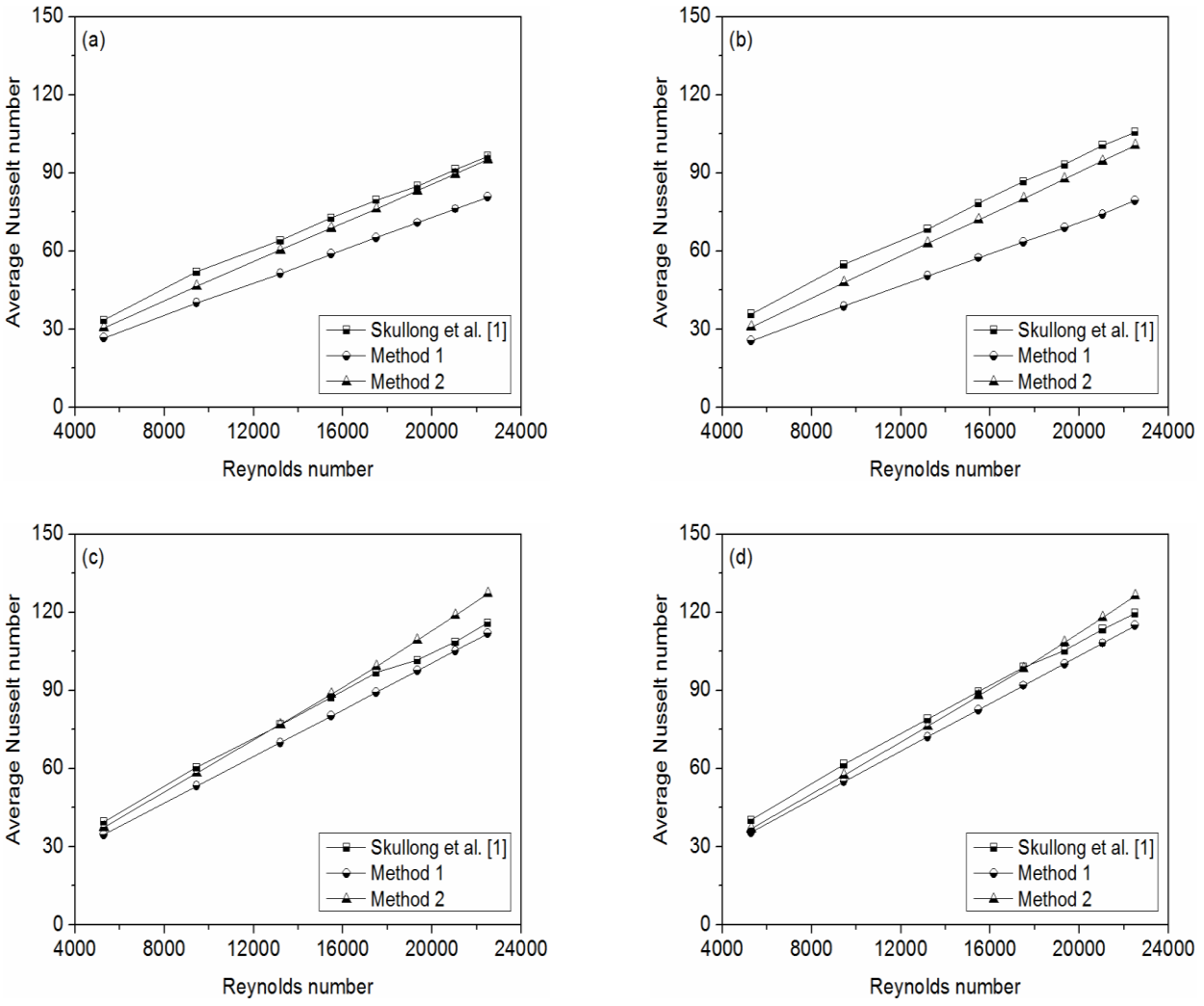

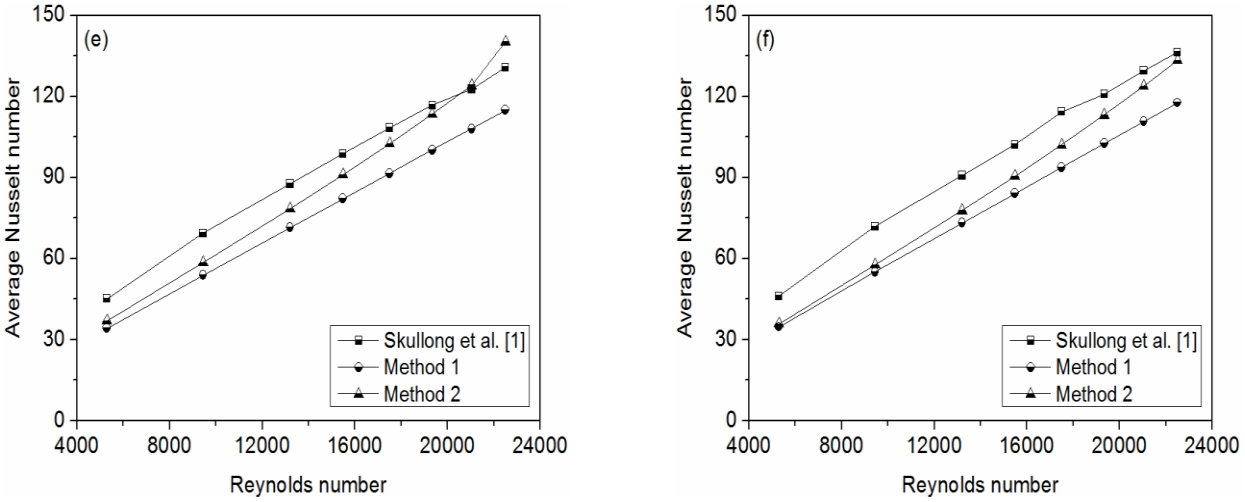

Fig. 4.4 Results of numerical analysis at different Reynolds number for (a) single square ribs, (b) single thin ribs, (c) staggered square ribs, (d) in-line square ribs, (e) staggered thin ribs and (f) in-line thin ribs.

The percentage deviation of numerical results using method-2 from experimental results of Skullong et al. [1] was found to be approximately 5, 8.3, 5, 7.4, 8.5 and 11.4 for solar air heaters with single square ribs, single thin ribs, staggered square ribs, in-line square ribs, staggered thin ribs and in-line thin ribs respectively.

Nusselt number calculated using method-1 was observed to be considerably lower than the experimental ones for all the case. The corresponding percentage deviations were calculated as 18.7, 27, 3.3, 7.4, 17 and 18.3 for solar air heaters with single square ribs, single thin ribs, staggered square ribs, in-line square ribs, staggered thin ribs and in-line thin ribs respectively.

4.2.3 Comparison of Nusselt number variation with Reynolds number for all the geometries

Fig. 4.5 graphically outlines a comparison between Nusselt number and Reynolds number for all the geometries. It can be inferred from the graph that there was a considerable augmentation in Nusselt number for both thin as well as square ribs. Interestingly, thin ribs gave much better thermal performance than their square counterparts. In-line gave the highest Nusselt number for the complete Reynolds number range used in this simulation. The possible reason attributed to this phenomenon is due to the strong interruption of flow and diversion of its direction by in-line thin baffles. The ribbed configurations in the increasing order of Nusselt number are single thin

ribs, single square ribs, staggered square ribs, in-line square ribs, thin staggered ribs and thin in-line ribs. The same pattern was observed in the experimental results of except that single thin ribs in the present work gave the lowest Nusselt numbers.

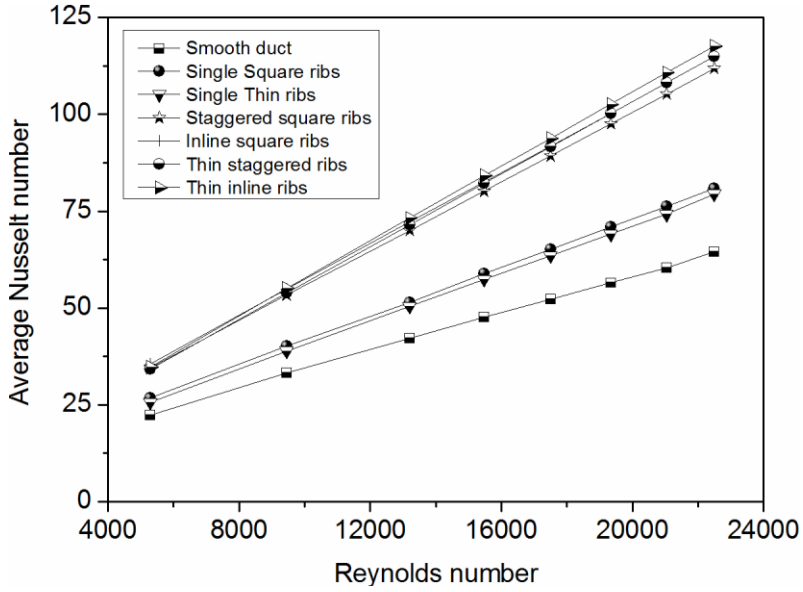

Fig. 4.5 Variation of Nu with Re for all the cases

4.2.4 Nusselt number enhancement (Nu/Nu_0) versus Reynolds number for separate geometries

Nusselt number enhancement ratio gives information about the increment in Nusselt number of a solar air heater with ribs from that of a smooth one. Fig. 4.6 gives a comparison Nusselt number enhancement alteration with Re for all the arrangements. In-line thin ribs yielded the best Nusselt number enhancement ratio. The maximum Nu/Nu_0 values with square ribs were 1.26, 1.74, 1.79 for single, staggered and in-line patterns respectively and those with thin ribs were 1.23, 1.79 and 1.83 respectively thereby clearly indicating that thin ribs have advantage over the square ones. The highest value of Nu/Nu_0 was observed for thin-in line ribs at Re = 21040. In the experimental work of Skullong et al. [1], the maximum Nu/Nu_0 values with square ribs were 1.52, 1.81 and 1.86 1.74 for single, staggered and in-line patterns respectively and those with thin ribs were 1.64, 2.05 and 2.13 respectively.

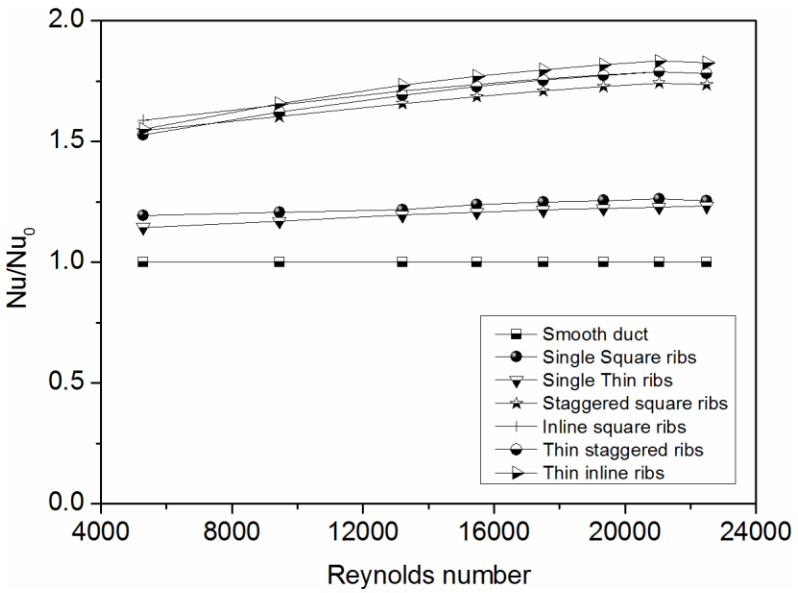

Fig. 4.6 Variation of Nu/Nu_0 with Re for all the cases

4.2.5 Local Nusselt number variation with length

The introduction of ribs leads to breakage of laminar leading to flow reattachment and separation in between the disturbances. Thin in-turn results in breaking of laminar sub-layer periodically thereby considerably augmenting the convective heat transfer. Local turbulence and flow mixing are caused due to the acceleration of flow between the tips of ribs. Fig. 4.7 represents local Nusselt number distribution with length for different cases at a Reynolds number of 15480.

Peaks in the graph can be observed at rib edges and at locations in between two consecutive ribs. It is further observed that the peaks are higher initially in the regions up-to 2-3 ribs and then these peaks become periodic along with invariable length reattachment lengths. Single peak between two consecutive ribs is observed for all the cases except that for staggered configurations where two peak points are observed. However the values at these peaks are lower than those of inline ribs, hence inline ribs gave higher convective heat transfer coefficients than their staggered counterparts.

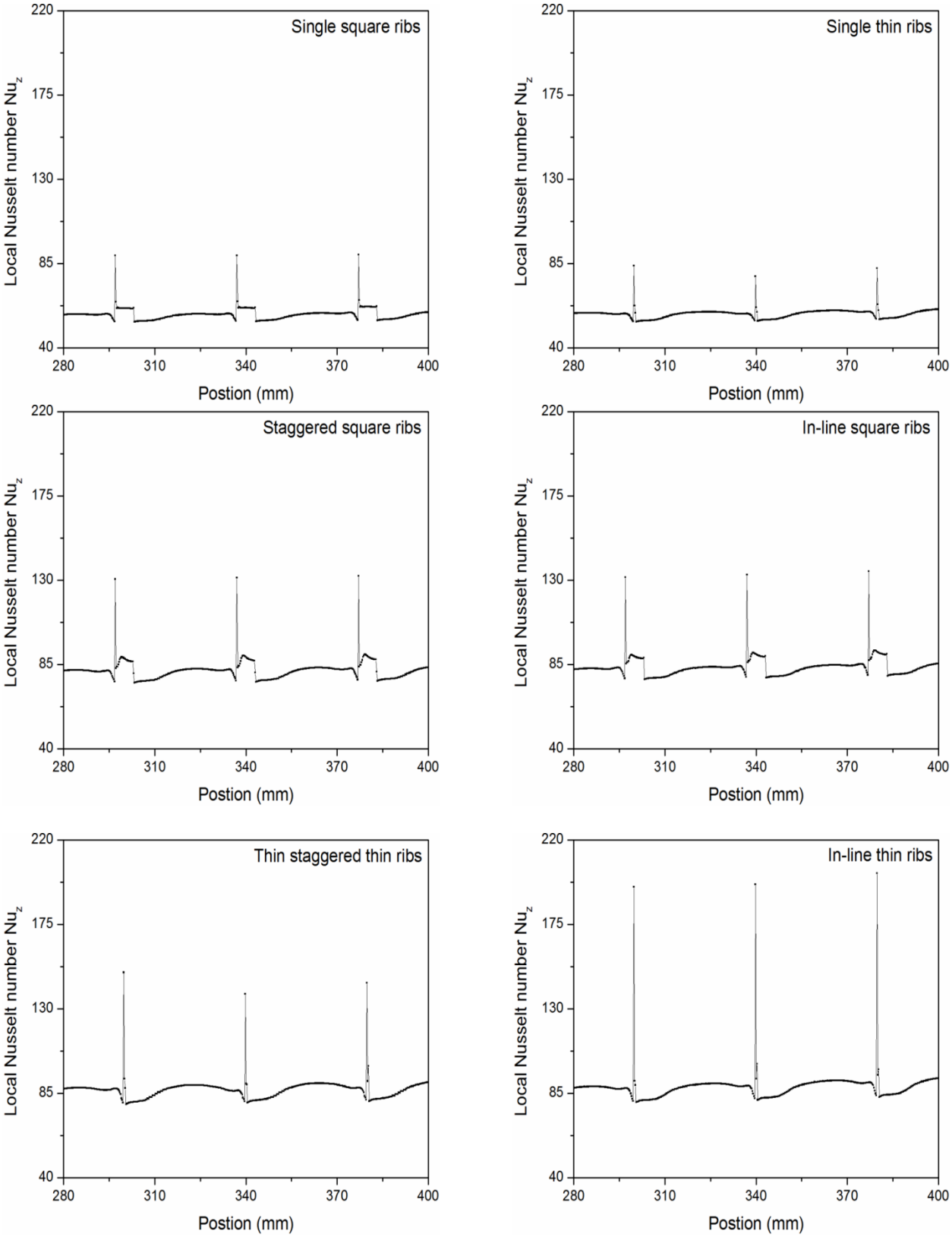

Fig. 4.7 Local Nusselt number variation with the length of test section for different arrangements of ribs

4.2.6 Velocity characteristics

Velocity vector contour plots at a Reynolds number of 5290 for different patterns are depicted in Fig. 4.8. There is an extreme irregularity in the contours of instantaneous velocity due to the effect of ribs. Eddy formation is clearly shown in the contours plot, in the vicinity of ribs. The fluid flow experiences sudden expansion leading to a separation region at the rib downstream. This separation is followed by reattachment of the fluid ahead the next rib. The periodic circulation of reattachment of flow leads to the formation of a small secondary vortex near the absorber plate and fluid junction.

The secondary vortices are much more strongly created in case of thin ribs. Furthermore it is observed that the velocity of the fluid is accelerated lengthwise as it passes through the test channel. Hence greater amount of disturbances are observed in the laminar sub layer thereby leading to a reduction in conductive transfer of heat and a significant augmentation in convective transfer of heat.

The formation of vortices and the stream line paths are exaggeratedly indicated in Fig. 4.8. The vortices are much stronger and bigger for in line configurations although there is more complexity in the velocity pattern in case of staggered rib patterns. Consequently, the heat transfer for in line ribs are slightly greater than that of staggered ribs.

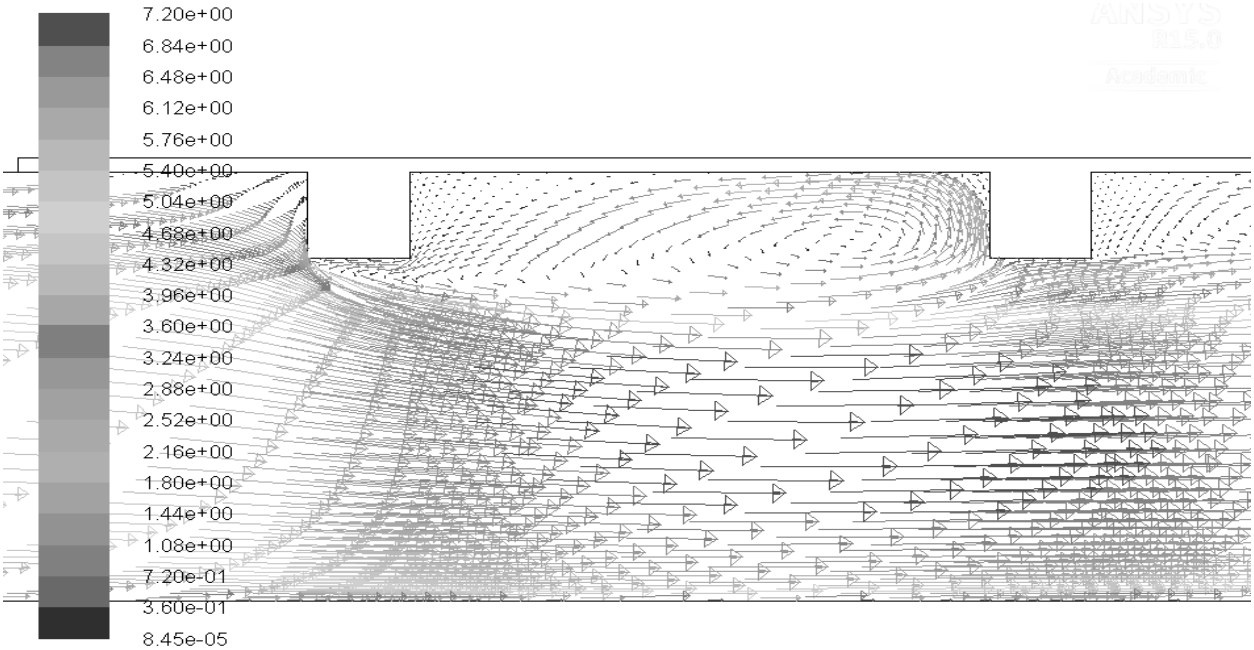

(a)

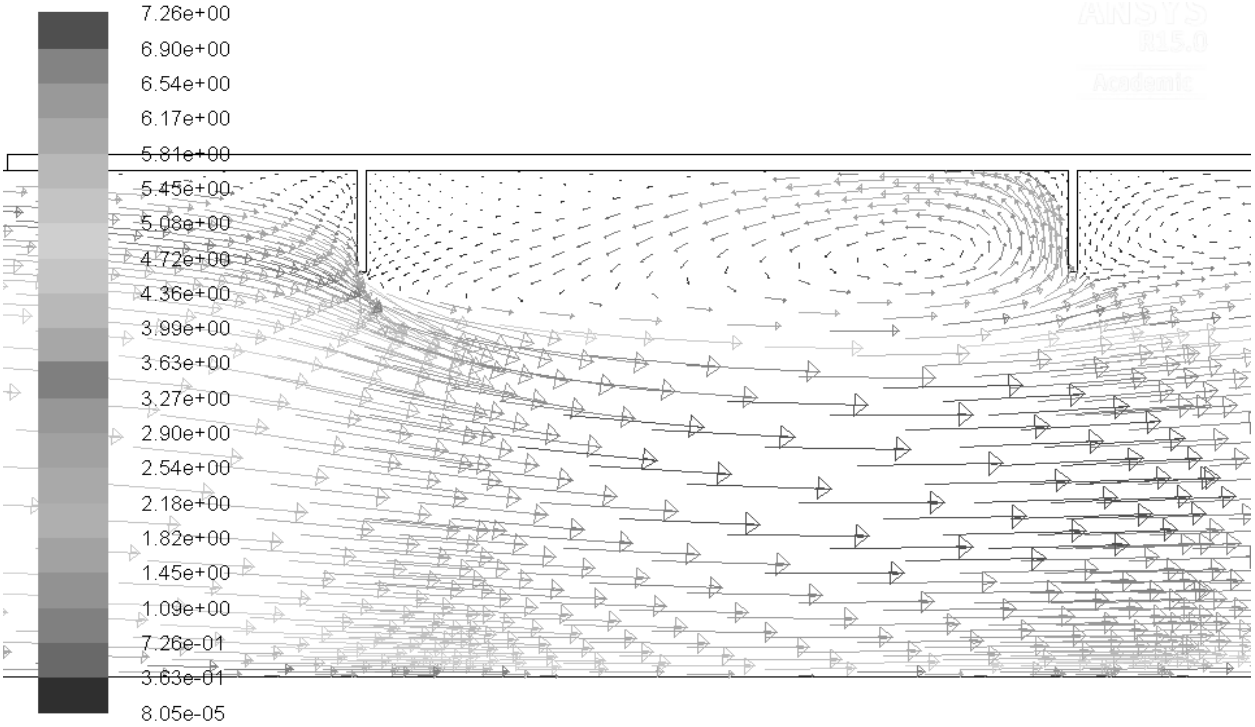
7.26e+00
6.90e+00
6.54e+00
6.17e+00
5.81e+00
5.45e+00
5.08e+00
4.72e+00
4.36e+00
3.99e+00
3.63e+00
3.27e+00
2.90e+00
2.54e+00
2.18e+00
1.82e+00
1.45e+00
1.09e+00
7.26e-01
3.63e-01
8.05e-05

(b)

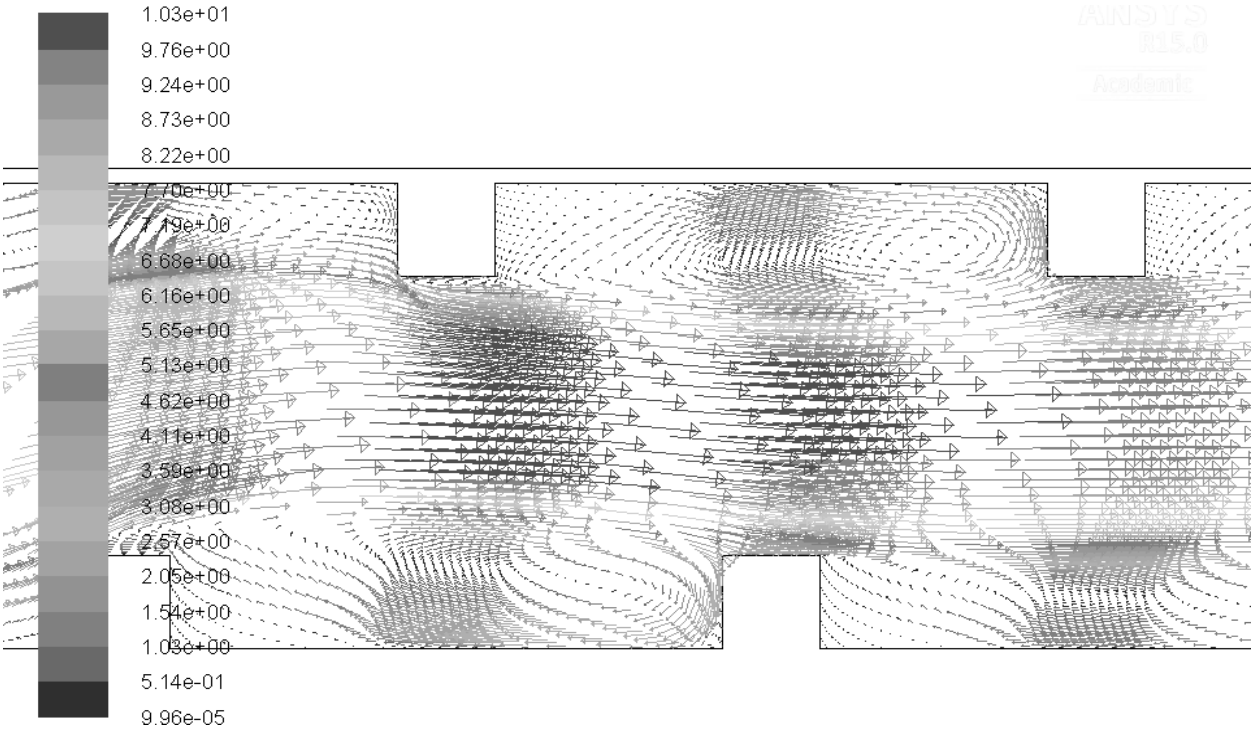
1.03e+01
9.76e+00
9.24e+00
8.73e+00
8.22e+00
7.70e+00
7.19e+00
6.68e+00
6.16e+00
5.65e+00
5.13e+00
4.62e+00
4.11e+00
3.59e+00
3.08e+00
2.57e+00
2.05e+00
1.54e+00
1.03e+00
5.14e-01
9.96e-05

(c)

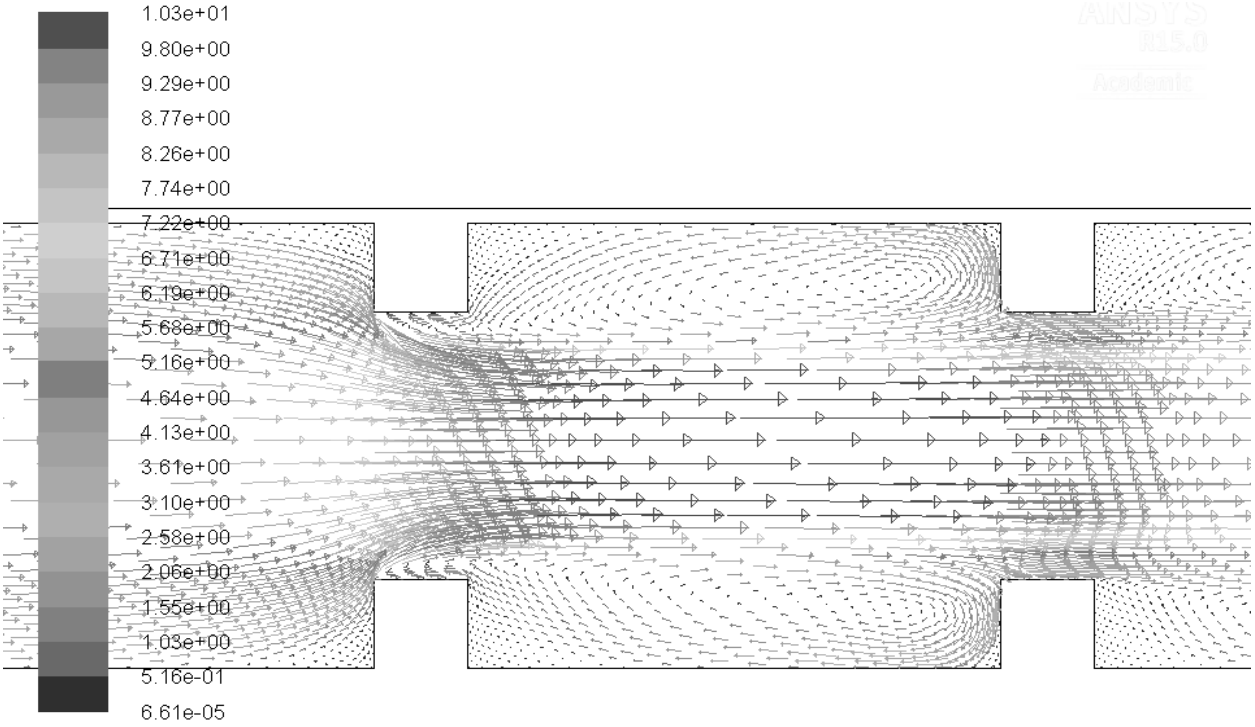
1.03e+01
9.80e+00
9.29e+00
8.77e+00
8.26e+00
7.74e+00
7.22e+00
6.71e+00
6.19e+00
5.68e+00
5.16e+00
4.64e+00
4.13e+00
3.61e+00
3.10e+00
2.58e+00
2.06e+00
1.55e+00
1.03e+00
5.16e-01
6.61e-05

(d)

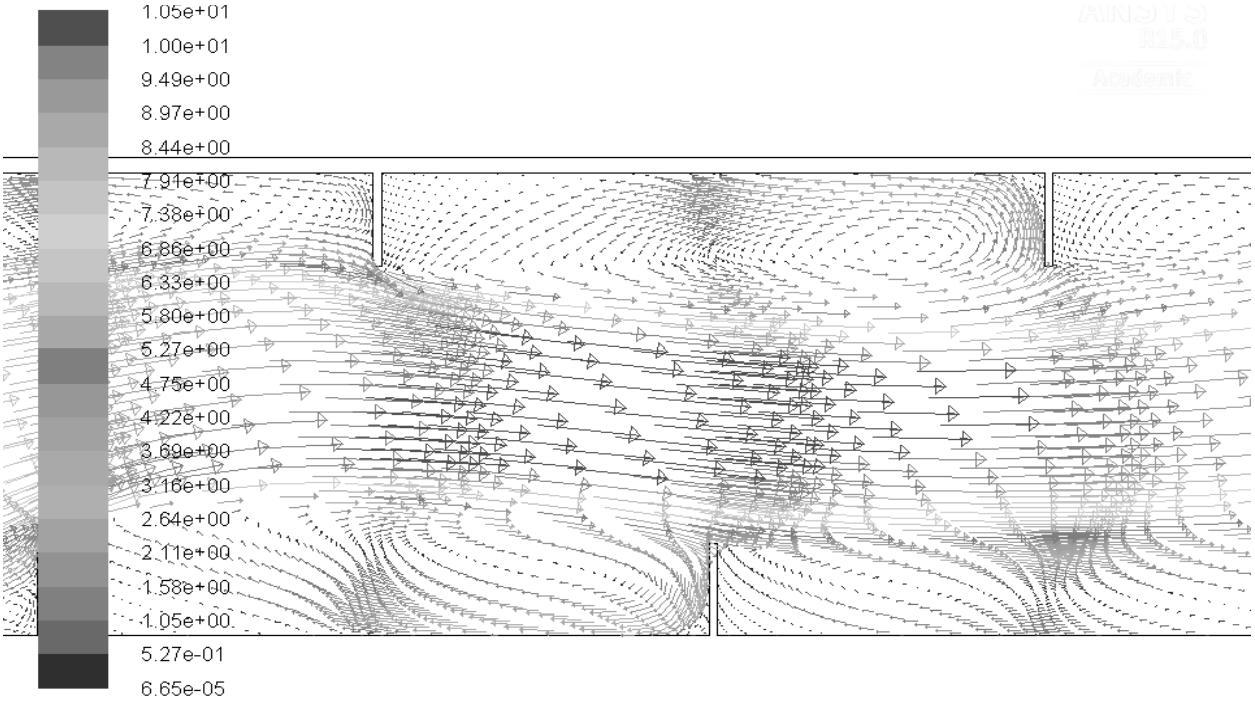
1.05e+01
1.00e+01
9.49e+00
8.97e+00
8.44e+00
7.91e+00
7.38e+00
6.86e+00
6.33e+00
5.80e+00
5.27e+00
4.75e+00
4.22e+00
3.69e+00
3.16e+00
2.64e+00
2.11e+00
1.58e+00
1.05e+00
5.27e-01
6.65e-05

(e)

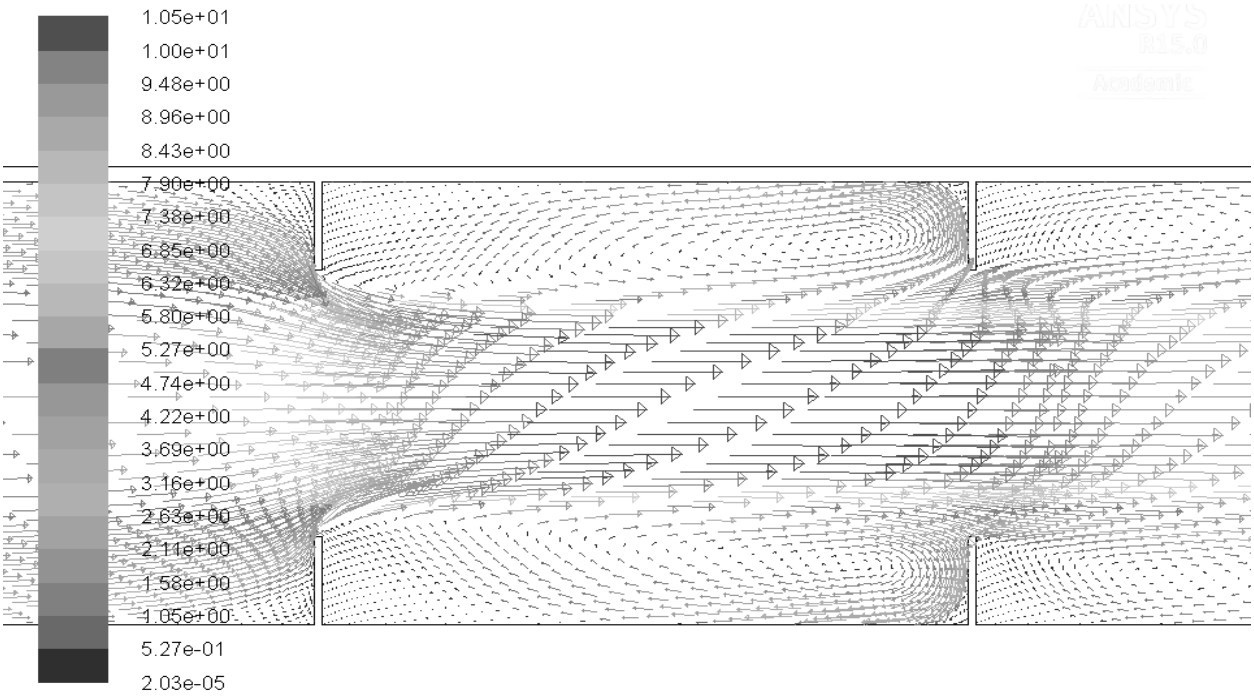

(f)

Fig. 4.8 Velocity vector contours of turbulent flow for (a) single square ribs, (b) single thin ribs, (c) staggered square ribs, (d) in-line square ribs, (e) staggered thin ribs and (f) in-line thin ribs.

Chapter 5

Conclusion and future scope

A two-dimensional numerical study was done to predict the influence of transverse rectangular cross-sectioned ribs on a solar air heater's convective heat transfer properties. A rectangular duct was constructed and numerical analysis was carried out on square and thin (high aspect ratio) rib shapes arranged in different fashion, namely single wall, staggered and in-line ribs arranged on two opposite walls including the absorber plate. Air was the working fluid and constant heat flux was applied only on the absorber plate's top surface. The output of numerical simulations drew the following conclusions

- On comparing simulation results, pertaining to smooth duct's average Nusselt number, for different turbulent models, it was found that SST-k-omega can best predict the thermal performance of the solar air heater.
- For all the cases considered in this study, increase in Reynolds number leads to augmentation in Nusselt number.
- When ribs/baffles are introduced just beneath the collector plate, there was a considerable alteration in the heat transfer coefficient of air.
- Two methods were used to calculate the average Nusselt number in which one method extracted the local Nusselt number at many points and on averaging these, gave the average Nusselt number and the other method resembled the one used in the existing experimental work. Good matching between existing experimental results and numerical outputs was spotted, when the second method was adopted to calculate the Nusselt number, thereby proving that CFD can be effectively applied for the design of solar air heaters. However the Nusselt number calculated using first method yielded values lower than the existing ones.
- The results revealed that the thin ribs yielded better performance than the squared ones. Similar results were also observed by Skullong et al. [1] in their experimental work.

- The staggered ribs gave lower Nusselt number than the in-line ones.
- Out of the three arrangements, the best thermal performance was given by thin inline ribs whose convective heat transfer coefficient was 1.83 times that of smooth duct.

Since, it was observed that high aspect ratio ribs allow higher convective heat transfer, hence it would be interesting to conduct research work on triangular shaped ribs having very low apex angles. The present work is expected to be very helpful for carrying out the new future project.

References

1. Skullong S., Thianpong C. and Promvonge, P., 2015, Effects of rib size and arrangement on forced convective heat transfer in a solar air heater channel, Heat and Mass Transfer, pp. 1-11.
2. Kalogirou, S. A., 2013, Solar energy engineering: processes and systems. Academic Press.
3. Yadav A. S. and Bhagoria J. L., 2013, Heat transfer and fluid flow analysis of solar air heater: a review of CFD approach, Renewable and Sustainable Energy Reviews, 23: pp. 60-79.
4. Sukhatme K. and Sukhatme S. P., 1996, Solar energy: principles of thermal collection and storage, Tata McGraw-Hill Education.
5. Twidell, J. and Weir, A. D., 2006, Renewable energy resources, Taylor & Francis.
6. Cengel Y. A. and Cimbala J. M., 2006, Fluid mechanics (Vol. 1), Tata McGraw-Hill Education.
7. Prasad K. and Mullick S. C., 1983, Heat transfer characteristics of a solar air heater used for drying purposes, Applied Energy, 13(2): pp. 83-93.
8. Prasad B. N. and Saini J. S., 1988, Effect of artificial roughness on heat transfer and friction factor in a solar air heater, Solar Energy, 41(6): pp. 555-560.
9. Prasad B. N. and Saini J. S., 1991, Optimal thermo-hydraulic performance of artificially roughened solar air heaters, Solar Energy, 47(2): pp. 91-96.
10. Liou T. M. and Hwang J. J., 1993, Effect of ridge shapes on turbulent heat transfer and friction in a rectangular channel, International Journal of Heat and Mass Transfer, 36(4): pp. 931-940.
11. Gupta D., Solanki S. C. and Saini J. S., 1993, Heat and fluid flow in rectangular solar air heater ducts having transverse rib roughness on absorber plates, Solar Energy, 51(1): pp. 31-37.
12. Saini R. P. and Saini J. S., 1997, Heat transfer and friction factor correlations for artificially roughened ducts with expanded metal mesh as roughness element, International Journal of Heat and Mass Transfer, 40(4): pp. 973-986.

13. Karwa R., Solanki, S. C. and Saini, J. S., 1999, Heat transfer coefficient and friction factor correlations for the transitional flow regime in rib-roughened rectangular ducts, International Journal of Heat and Mass Transfer, 42(9): pp. 1597-1615.
14. Verma S. K. and Prasad B. N., 2000, Investigation for the optimal thermos-hydraulic performance of artificially roughened solar air heaters, Renewable Energy, 20(1): pp. 19-36.
15. Murata A. and Mochizuki S., 2001, Comparison between laminar and turbulent heat transfer in a stationary square duct with transverse or angled rib turbulators, International Journal of Heat and Mass Transfer, 44(6): pp. 1127-1141.
16. Ahn S. W., 2001, The effects of roughness types on friction factors and heat transfer in roughened rectangular duct, International Communications in Heat and Mass Transfer, 28(7): pp. 933-942.
17. Momin A. M. E., Saini J. S. and Solanki S. C., 2002, Heat transfer and friction in solar air heater duct with V-shaped rib roughness on absorber plate, International Journal of Heat and Mass Transfer, 45(16): pp. 3383-3396.
18. Chandra P. R., Alexander C. R. and Han J. C., 2003, Heat transfer and friction behaviors in rectangular channels with varying number of ribbed walls. International Journal of Heat and Mass Transfer, 46(3): pp. 481-495.
19. Tanda G., 2004, Heat transfer in rectangular channels with transverse and V-shaped broken ribs, International Journal of Heat and Mass Transfer, 47(2): pp. 229-243.
20. Sahu M. M. and Bhagoria J. L., 2005, Augmentation of heat transfer coefficient by using 90 broken transverse ribs on absorber plate of solar air heater, Renewable Energy, 30(13): pp. 2057-2073.
21. Chang S. W., Liou T. M. and Lu M. H., 2005, Heat transfer of rectangular narrow channel with two opposite scale-roughened walls, International Journal of Heat and Mass Transfer, 48(19): pp. 3921-3931.
22. Bhagoria J. L., Saini J. S. and Solanki S. C., 2002, Heat transfer coefficient and friction factor correlations for rectangular solar air heater duct having transverse wedge shaped rib roughness on the absorber plate, Renewable Energy, 25(3): pp. 341-369.
23. Chaube A., Sahoo P. K. and Solanki S. C., 2006, Analysis of heat transfer augmentation and flow characteristics due to rib roughness over absorber plate of a solar air heater, Renewable Energy, 31(3): pp. 317-331.

24. Jaurker A. R., Saini J. S. and Gandhi B. K., 2006, Heat transfer and friction characteristics of rectangular solar air heater duct using rib-grooved artificial roughness, Solar Energy, 80(8): pp. 895-907.
25. Wang C., Guan Z., Zhao X. and Wang D., 2006, Numerical simulation study on transpired solar air collector, Renewable Energy Resources and a Greener Future, Vol. VIII-3-4
26. Karmare S. V. and Tikekar A. N., 2007, Heat transfer and friction factor correlation for artificially roughened duct with metal grit ribs, International Journal of Heat and Mass Transfer, 50(21): pp. 4342-4351.
27. Layek A., Saini J. S. and Solanki S. C., 2007, Second law optimization of a solar air heater having chamfered rib–groove roughness on absorber plate, Renewable Energy, 32(12): pp. 1967-1980.
28. Aharwal K. R., Gandhi B. K. and Saini J. S., 2008, Experimental investigation on heat-transfer enhancement due to a gap in an inclined continuous rib arrangement in a rectangular duct of solar air heater, Renewable Energy, 33(4): pp. 585-596.
29. Promvonge P. and Thianpong C, 2008, Thermal performance assessment of turbulent channel flows over different shaped ribs, International Communications in Heat and Mass Transfer, 35(10): pp. 1327-1334.
30. Saini S. K. and Saini R. P., 2008, Development of correlations for Nusselt number and friction factor for solar air heater with roughened duct having arc-shaped wire as artificial roughness, Solar Energy, 82(12): pp. 1118-1130.
31. Saini R. P. and Verma J., 2008, Heat transfer and friction factor correlations for a duct having dimple-shape artificial roughness for solar air heaters. Energy, 33(8): pp. 1277-1287.
32. Saini, R. P. and Singal S. K., 2008, Investigation of thermal performance of solar air heater having roughness elements as a combination of inclined and transverse ribs on the absorber plate, Renewable Energy, 33(6): pp. 1398-1405.
33. Thianpong C., Chompookham T., Skullong S. and Promvonge P., 2009, Thermal characterization of turbulent flow in a channel with isosceles triangular ribs, International Communications in Heat and Mass Transfer, 36(7): pp. 712-717.
34. Kumar S. and Saini R. P., 2009, CFD based performance analysis of a solar air heater duct provided with artificial roughness, Renewable Energy, 34(5): pp. 1285-1291.

35. Kumar A., Bhagoria, J. L. and Sarviya R. M., 2009, Heat transfer and friction correlations for artificially roughened solar air heater duct with discrete W-shaped ribs, Energy Conversion and Management, 50(8): pp. 2106-2117.
36. Chompookham T., Thianpong C., Kwankaomeng S. and Promvonge P., 2010, Heat transfer augmentation in a wedge-ribbed channel using winglet vortex generators, International Communications in Heat and Mass Transfer, 37(2): pp. 163-169.
37. Karmare S. V. and Tikekar A. N., 2010, Analysis of fluid flow and heat transfer in a rib grit roughened surface solar air heater using CFD, Solar Energy, 84(3): pp. 409-417.
38. Promvonge P., Changcharoen W., Kwankaomeng S. and Thianpong C., 2011, Numerical heat transfer study of turbulent square-duct flow through inline V-shaped discrete ribs. International Communications in Heat and Mass Transfer, 38(10): pp. 1392-1399.
39. Sethi M. and Thakur N. S., 2012, Correlations for solar air heater duct with dimpled shape roughness elements on absorber plate, Solar Energy, 86(9): pp. 2852-2861.
40. Sriromreun P., Thianpong C. and Promvonge P., 2012, Experimental and numerical study on heat transfer enhancement in a channel with Z-shaped baffles, International Communications in Heat and Mass Transfer, 39(7): pp. 945-952.
41. Promvonge P., Skullong S., Kwankaomeng S. and Thiangpong C., 2012, Heat transfer in square duct fitted diagonally with angle-finned tape-Part 1: Experimental study, International Communications in Heat and Mass Transfer, 39(5): pp. 617-624.
42. Promvonge P., Skullong S., Kwankaomeng S. and Thiangpong C., 2012, Heat transfer in square duct fitted diagonally with angle-finned tape-Part 2: Numerical study, International Communications in Heat and Mass Transfer, 39(5): pp. 625-633.
43. Kumar A., Saini R. P. and Saini J. S., 2012, Heat and fluid flow characteristics of roughened solar air heater ducts–A review, Renewable Energy, 47: pp. 77-94.
44. Yadav A. S. and Bhagoria J. L., 2013, A CFD (computational fluid dynamics) based heat transfer and fluid flow analysis of a solar air heater provided with circular transverse wire rib roughness on the absorber plate, Energy, 55: pp. 1127-1142.
45. Yadav A. S. and Bhagoria J. L., 2014, A numerical investigation of square sectioned transverse rib roughened solar air heater, International Journal of Thermal Sciences, 79: pp. 111-131.

46. Prasad B. N., Behura A. K. and Prasad L., 2014, Fluid flow and heat transfer analysis for heat transfer enhancement in three sided artificially roughened solar air heater, Solar Energy, 105: pp. 27-35.
47. Aharwal K. R., Pawar C. B. and Chaube, A., 2014, Heat transfer and fluid flow analysis of artificially roughened ducts having rib and groove roughness, Heat and Mass Transfer, 50(6): pp. 835-847.
48. Tamna S., Skullong S., Thianpong C. and Promvonge P., 2014, Heat transfer behaviors in a solar air heater channel with multiple V-baffle vortex generators, Solar Energy, 110: pp. 720-735.
49. Skullong S., Kwankaomeng S., Thianpong C. and Promvonge P., 2014, Thermal performance of turbulent flow in a solar air heater channel with rib-groove turbulators, International Communications in Heat and Mass Transfer, 50: pp. 34-43.